

**A RAMAN CELL BASED ON HOLLOW CORE PHOTONIC CRYSTAL FIBRE
FOR HUMAN BREATH ANALYSIS**

by

Kam Kong Chow

A THESIS SUBMITTED IN PARTIAL FULFILLMENT OF
THE REQUIREMENTS FOR THE DEGREE OF

MASTER OF SCIENCE

in

THE FACULTY OF GRADUATE STUDIES

(Physics)

THE UNIVERSITY OF BRITISH COLUMBIA

(Vancouver)

November 2012

© Kam Kong Chow, 2012

Abstract

Lung cancer is the top cancer killer in Canada and North America. Current lung cancer detection tools involving X-ray, CT and bronchoscopy are relatively time-consuming and costly. Breath analyses done by mass spectrometry have shown that certain endogenous volatile organic compounds (VOCs) are related to lung cancer and revealed the potential of breath analysis for lung cancer detection. But mass spectrometry is costly and has slow turnaround times. Raman spectroscopy is a promising candidate for breath analysis because it can offer unique fingerprint-type signals for molecular identification. Hollow core-photonic crystal fibre (HC-PCF) is a novel light guide which allows light to be guided in a small hollow core and it can be filled with a gaseous sample (i.e., human breath) for spectral analysis. Our objective is to develop a simple, cost-effective and non-invasive tool based on Raman spectroscopy for breath analysis and potentially lung cancer screening.

A Raman-gas analyzer was designed, based on photonics technology. A gas supply system was built to provide a sealed environment for the loading and unloading of gaseous samples. A laser source at 785 nm was used as the pump for molecular excitation. Stokes Raman signals generated in the hollow core of the HC-PCF can be guided by collection optics and analyzed by a Raman spectrometer. Raman spectra have been obtained successfully from air, reference gases (hydrogen gas, oxygen gas, carbon dioxide gas), and human breath. The limit of detection of the system was found to be approximately 15 parts per million by CO₂ concentration in the ambient air, characterized by the Raman peaks at 1286 cm⁻¹ and 1388 cm⁻¹. This is more than a 100-fold improvement over the recently reported detection limit

with a reflective capillary fibre-based Raman cell. Furthermore the detection limit can be further improved by changes to the optical configurations, optimizing the interaction length of the HC-PCF and possible pre-concentration method to enhance signal-to-noise ratio. This work demonstrated a working prototype of a simple, compact, and cost-effective Raman-gas analyzer based on hollow core photonic crystal fibre, which could potentially be used for lung cancer screening through breath analysis.

Table of Contents

Abstract.....	ii
Table of Contents	iv
List of Tables	vii
List of Figures.....	viii
List of Abbreviations	x
Acknowledgements	xii
Dedication	xiv
Chapter 1: Introduction	1
1.1 Lung cancer and its screening methods	1
1.1.1 Anatomy of the lung	1
1.1.2 Lung cancer.....	1
1.1.3 Current lung cancer screening methods	3
1.2 Review of human breath and its analyses for lung cancer.....	5
1.2.1 Physiology of human breath	5
1.2.2 Background of breath analysis.....	6
1.2.3 Exhaled biomarkers and lung cancer related VOCs	7
1.2.4 Current human breath analysis techniques	10
1.2.4.1 Mass spectrometry-related techniques for breath analysis	11
1.2.4.2 Laser absorption spectrometry-related techniques for breath analysis	13
1.3 Raman scattering and fibre optics.....	15
1.3.1 Raman scattering.....	15

1.3.2	Fibre optics.....	18
1.3.2.1	Conventional optical fibres	18
1.3.2.2	Photonic crystal fibres (PCF).....	19
1.3.3	Raman scattering in HC-PCF.....	20
1.4	Hypothesis and objective	22
Chapter 2: System development.....		25
2.1	System overview	25
2.2	HC-PCF.....	28
2.3	Gas chamber and tubing system	30
Chapter 3: Results and analysis.....		33
3.1	The measurements of reference gases.....	33
3.1.1	The measurement of oxygen gas.....	33
3.1.2	The measurement of hydrogen gas	34
3.1.3	The measurement of carbon dioxide gas	35
3.2	The measurements of breath and ambient air	36
3.2.1	The measurement of human exhaled breath	36
3.2.2	The measurements of the ambient air	37
3.3	Signal-to-noise ratio.....	39
Chapter 4: Discussion and conclusion.....		41
4.1	Comparison of a HC-PCF based Raman breath analyzer to that of based on a hollow capillary fibre.....	41
4.2	Future work to improve the device sensitivity.....	45
4.3	Predicted challenges in breath analysis for clinical application	47

4.4	Conclusion	50
	References	51

List of Tables

Table 1 Specifications of the HC-800-01 HC-PCF (sourced from the manufacturer's datasheet)	28
Table 2 Comparison between our HC-PCF-based Raman breath analyzer to that of based on a hollow capillary fibre reported by Y. Okita et al.	44

List of Figures

Figure 1 Examples of potential lung cancer-related breath biomarkers. Frequencies represent the number of papers citing each compound (27, 35-37, 39-45).....	9
Figure 2 Energy level transitional schemes showing Rayleigh scattering, Stokes scattering and anti-Stokes scattering. 0, 1, 2... are the ground state and subsequent vibrational states of the molecule.....	17
Figure 3 Illustration of a) light ray transmission in the fibre core, b) cross-sectional structure of an optical fibre.....	19
Figure 4 Comparison of a laser beam a) focused to free space (no light guide); b) focused to a high attenuation hollow tube with inner reflective coating (thickness of the arrows represent the intensity of the light rays); c) focused to a low attenuation HC-PCF.....	22
Figure 5 Schematic diagram of the Raman-gas cell system.....	27
Figure 6 Cross-sectional view of HC-800-01 under a 20x microscope objective.....	29
Figure 7 Schematic diagram of the gas chamber design.....	31
Figure 8 The measured vibrational and rotational spectrum of the pure oxygen gas by the Raman cell.....	34
Figure 9 The measured rotational Raman spectrum of the pure hydrogen gas by the Raman cell.....	35
Figure 10 The measured vibrational Raman spectrum of the carbon dioxide gas by the Raman cell.....	36
Figure 11 The measured human exhaled breath spectrum by the Raman cell showing Raman features of the carbon dioxide and oxygen molecules.....	37

Figure 12 The measured spectrum of the ambient air by the Raman cell showing the Raman features of the oxygen gas..... 38

Figure 13 The measured spectrum of the ambient air by the Raman cell showing the Raman features of the carbon dioxide gas and a portion of the rotational oxygen lines 39

Figure 14 An enlarged Raman spectrum by the Raman cell showing the carbon dioxide features in the ambient air with error bars assigned 40

List of Abbreviations

CCD	Charge-coupled device
CRDS	Cavity ring down spectroscopy
CW	Continuous wave
eCO ₂	Exhaled CO ₂
eO ₂	Exhaled O ₂
GC	Gas chromatography
GC-MS	Gas chromatography-mass spectrometry
HC-PCF	Hollow core-photonic crystal fibre
LAS	Laser absorption spectroscopy
m/z	Mass-to-charge
MS	Mass spectrometry
NA	Numerical aperture
NPT	National pipe thread
NSCLC	Non-small cell lung carcinoma
PAS	Photoacoustic spectroscopy
PC	Photonic crystal
PCF	Photonic crystal fibre
ppbv	Parts per billion per volume
ppmv	Parts per million per volume
pptv	Parts per trillion per volume
PTR-MS	Proton transfer reaction-mass spectrometer

SCLC	Small cell lung carcinoma
SIFT-MS	Selected ion flow tube-mass spectrometer
SPME	Solid-phase microextraction
TDLAS	Tunable diode laser absorption spectroscopy
VOCs	Volatile organic compounds

Acknowledgements

I would like to express my deepest gratitude to my supervisor Dr. Haishan Zeng, Distinguished Scientist in the Integrative Oncology Department – Imaging Unit, BC Cancer Agency. I thank Dr. Zeng for providing guidance through my graduate study, both academically and financially. His wide knowledge in the field has encouraged and inspired my interest and knowledge in the Biophotonics industry.

I would like to thank the Canadian Cancer Society for funding support in this project.

I wish to express my particular thanks to Dr. Michael A. Short for enlarging my vision of science and providing coherent answers to my endless questions. His logical way of thinking has been of great value for me. His understanding, encouraging and personal guidance have provided a good basis of this thesis.

I warmly thank Dr. Jianhua Zhao for his constructive comments and support throughout my Master's study.

I offer my enduring gratitude to the faculty, staff and my fellow students at UBC who have inspired me to continue my work in this field.

I wish to thank my co-workers in the BC Cancer Agency: Mark Cardeno, Priscilla Fung, Jagoda Korbelik, Dr. Stephen Lam, Sylvia Lam, Dr. Pierre Lane, Dr. Anthony Lee, Myles McKinnon, Brent Sutherland.

I thank my fellow graduate students in the Integrative Oncology Department: Keith Hau, Gerald Li, Hanna Pawluk, Simon Shen, Giselle Tian, Tracy Wang, Edward Yu.

Dedication

To my parents, families and friends

Chapter 1: Introduction

In this introductory chapter, the current status of lung cancer and its screening methods, the history and current status of breath analysis and the potential of Raman spectroscopy serving as a breath analyzer will be reviewed.

1.1 Lung cancer and its screening methods

1.1.1 Anatomy of the lung

The lungs are essential organs in our respiratory system and gases are exchanged through breathing to keep one alive. It is located at the thoracic cavity and is composed of three lobes on the right and two on the left, which are all connected by the trachea and bronchi. When the air is inhaled, it passes through the nose or mouth to the windpipe and then divides into two bronchi to the left or right lung. Each of the bronchi branches into bronchioles and terminates at numerous alveoli. An alveolus is an air cavity supported by thin and elastic membranes to separate blood capillaries and inhaled air. This boundary allows gases to diffuse across the membrane between the blood capillaries and inhaled air. It has been estimated that there are over 300 million of alveoli in the lung. The alveolar surface area of an adult human can vary from 97 to 194 m² with a mean of 143 m², which is about half the size of a standard tennis court (1, 2).

1.1.2 Lung cancer

Cancer, as defined by the World Health Organization (WHO), is a generic term describing a group of diseases in any part of the body such that abnormal cells grow uncontrollably, beyond the usual boundaries and invade other parts of the body (3). Lung cancer is the top

killer among all types of cancer worldwide in 2008 (3). In 2011, there were estimated over 150,000 deaths related to cancers of the lung and bronchus in the United States, which is higher than colon, stomach, liver and pancreas cancer deaths combined (4). Cancers that begin in the lungs are called lung cancer and it most commonly develops from excessive growth of the epithelial cells. There are mainly two types of lung cancers, small cell lung carcinoma (SCLC) and non-small cell lung carcinoma (NSCLC).

The cells of SCLC contain dense granules which are neuroendocrine hormones (13-15%) and the majority of SCLC is related to smoking (5, 6). SCLC cells are small and often start in the bronchi but they can reproduce fairly quickly and form large tumours (7). NSCLC is the most common type of lung cancer, around 80% (8) of lung cancer patients are diagnosed with NSCLC. NSCLC is any type of epithelial lung cancer other than SCLC. There are three main subtypes of NSCLC: adenocarcinoma (25-35%), squamous cell lung carcinoma (30-35%), and large cell lung carcinoma (10-15%) (6). Although there are 10-15% of patients who are non-smokers with unknown causes of NSCLC development, tobacco is believed to be the major cause of lung cancer (9). Other reasons include air pollutants and family history.

When smoke particles are inhaled to the lung, certain free radicals may be sensitive to the lung tissues. Those free radicals may cause DNA damage and transformation. The transformed and survived cells then start to grow but differ from healthy lung tissues. The high proliferation rate of those cells leads to the fast-growing rate of tumours. Malignant lung tumours can grow uncontrollably, as a result, airway passages in the lung may be blocked due to local tumour. Bleeding may also occur and then coughed up to cause blood-stained

sputum. Survival rates of lung cancer remain low since most cases are diagnosed in advanced stage as the symptoms such as blood-stained sputum and breathing difficulty do not usually happen in early-stage lung cancer (10). About 25% of lung cancer patients have no obvious symptoms and are detected incidentally during health check (6). In advanced stage lung cancer cases, metastatic lung cancer in other organs in the body is common, such as the liver, bone and brain. In fact, half of all lung cancer patients have distant metastases at the time of diagnosis (11). This may cause multiple cancer complications and makes lung cancer more difficult to treat. The prognosis of lung cancer patients with metastasis is poor, and the 5-year survival rate of lung cancer patient with metastasis at the time of diagnosis is less than 1% (6). If lung cancer can be diagnosed and treated while it remains local, the five-year survival rate can increase to over 50% (12). This shows that effective screening tests for lung cancer in early stages, which is more likely to be treatable, would greatly improve the survival rates of lung cancer patients.

1.1.3 Current lung cancer screening methods

Screening refers to simple medical tests to help find diseased individuals from the asymptomatic public. Follow-up diagnostic tests are typically needed for confirmation (13). A successful screening tool should be able to reduce the mortality rate of the disease with the least degree of pain and invasiveness together with reasonable clinical sensitivity, specificity and cost (14, 15). Chest X-ray is one of the most common lung cancer initial imaging tests and it is often useful for discovering small resectable tumours, but chest x-rays do not reduce the number of new advanced stage lung cancer cases nor the mortality (15). CT gives more anatomic information that may be useful to provide guidance for the needle biopsy. But the

high cost, slow turnaround time and radiation exposure of CT make it less ideal for lung cancer screening. Sputum cytology analysis is the least invasive test for lung cancer. Sputum is usually obtained from conscious patients with cough, but induced sputum is considered somewhat invasive and uncomfortable. Sputum can contain high concentrations of malignant cells but varies significantly according to the tumour location. It performs best with central tumours, but less effective with peripheral cancers (16). Bronchoscopy is important for staging and it can be a diagnostic tool for lung cancer with integrated biopsy forceps to perform needleless biopsy sampling. Autofluorescence bronchoscopy makes use of the fluorescence properties of tissues to locate malignant lesions with higher sensitivity than using white light, but generally lacks specificity (17). More invasive procedures are sometimes indicated such as the open lung biopsy, when less invasive diagnostic tools do not work. Most of the aforementioned tools are not very useful for screening to reduce mortality (18, 19). Currently, there is no lung cancer screening tool generally accepted by health professions as they are usually costly, inefficient and considerably invasive, which causes long waiting time to patients and places a burden to the health care system (19). Some are considered as ineffective because of the high false-positive rates and cause unnecessary invasive confirmation tests to verify the results. A low cost, efficient and non-invasive lung cancer screening tool would be a great advancement in lung cancer control. Breath tests have been recognized as a promising candidate for lung cancer screening (6).

1.2 Review of human breath and its analyses for lung cancer

1.2.1 Physiology of human breath

Breathing is a major process in the body to perform gas exchange. For example, homeostatic processes maintain a constant condition of oxy- and deoxyhemoglobin concentrations. The body needs oxygen and sugar to provide energy to stay alive. In cellular respiration, oxygen is consumed and carbon dioxide is produced as waste. Red blood cells transport and deliver these dissolved gases to and from cells in our body via blood flow. Gas exchange takes place in the lung, more precisely at the alveolar membranes. A human exhaled breath (tidal volume) can be generally separated into two parts. The first part is called the dead space air, roughly 150 ml for a healthy subject, where inhaled air is trapped in upper airway and there is no gas exchange between blood and breath air. Alveolar breath is roughly 350 ml of gases which comes from the lung where gas exchange has taken place (20).

There are three basic processes of respiration: Ventilation is the first part of respiration which involves inhalation and exhalation. Ventilation is coordinated by contraction and relaxation of the diaphragm and intercostal muscles located at the rib cage. Air is inhaled from the nose and mouth followed by the airways and reaches alveoli by the pressure difference created by the change of lung volume. External respiration is the second part of the respiration process, in which gases are exchanged at the alveolar membranes. Gases are exchanged through the walls of numerous small air sacs and to the blood capillaries. Molecules that dissolved in blood will then be brought to other parts of the body by the circulatory system. The released carbon dioxide and left over molecules in air are then exhaled back to the atmosphere by the

same route that they were inhaled. The third part is called internal respiration which describes the gas exchange between the body cells and blood (1).

1.2.2 Background of breath analysis

In the ancient days Hippocrates instructed students to smell patients' breaths. For example, a fruity smelling breath can mean high risk of diabetes and a fishy smelling breath may point the finger to liver impairment (21). The inhaled dry air composition by volume is approximately 78% N₂, 21% O₂ and 0.03% CO₂, and other trace components. Human exhaled breath usually contains approximately 78% N₂, 16% O₂ and 4% CO₂ and other substances in trace amounts that vary from person to person (22, 23).

The first detailed quantitative study of human breath analysis was in the 1970s using gas chromatography (GC) by Pauling et al (24). After Pauling's finding, Phillips et al stated that there are over three thousand different substances in human exhaled breath (25). These substances, which constitute a distinctive "breathprint," are in trace amounts and occur because of various biochemical processes in human body. By correctly analyzing the exhaled "breathprint", the physiological status of the body can be revealed and provide results quicker than the conventional body fluid tests (20, 26).

Blood and urine tests both have been serving the medical industry for years. Scientists and physicians have been relying on these body fluid tests to check the status of the human body such as disease diagnosis, drug tests, etc. However, these reliable techniques require sample collection, which some consider as invasive and inconvenient, and are not suitable for on-line

monitoring. Furthermore, off-line sampling is considered as relatively time-consuming since it requires extra work for analysis. Breath analysis has the potential to benefit the medical service as it can provide point-of-care, cost-effective and painless means to routine clinical tests and monitoring.

1.2.3 Exhaled biomarkers and lung cancer related VOCs

Volatile compounds are chemical compounds that have low melting and boiling points under atmospheric pressure. Studies have shown that volatile compounds can be important indicators of metabolic status and biomarkers of diseases to distinguish healthy and diseased state (24, 27-31). Volatile compounds are known to appear in blood and to be able to cross the alveolar membrane in the lung and thus be present in expired breath. This makes breath analysis a promising tool to serve in disease screening/diagnosis (29, 32), drug assay/monitoring (33), cancer screening/detection (34-37), monitoring patients at surgery (33), etc.

Volatile organic compounds (VOCs) are a subset of volatile compounds which are organic, such as benzene and isoprene. VOCs can be found in exhaled breath in the range of parts per trillion to parts per million by volume (pptv to ppmv), from the environmental cycle and production in the human body. Measuring endogenous VOCs can be useful to monitor the biochemical processes of the body and it is believed that the products of the biochemical processes of patients with and without lung cancer can be different and therefore distinguishable by breath analysis (38). This field has been interesting to researchers since

there has been an overwhelming need to offer efficient, non-invasive and sensitive screening tools for patients in early-stage lung cancer to reduce mortality.

By examining the breath collected from lung cancer patients and control groups, experimental studies have suggested biomarkers for lung cancer screening, as listed in Figure 1 (27, 35-37, 39-45). Most of the early findings of exhaled components were verified by mass spectrometry-based tools, because of their strong analytical power in molecular identification. However, researchers generally do not obtain consistent results. There are over 50 different lung cancer-related VOCs suggested in ten publications from 1999 to 2010, with between 2 and 22 VOCs per study. The exhaled biomarkers of lung cancer have long been studied, however there is a lack of solid evidence to correlate these chemicals to lung cancer. The inconsistency of lung cancer biomarkers could be due to collection method, location and diet, etc, which are discussed in section 4.3.

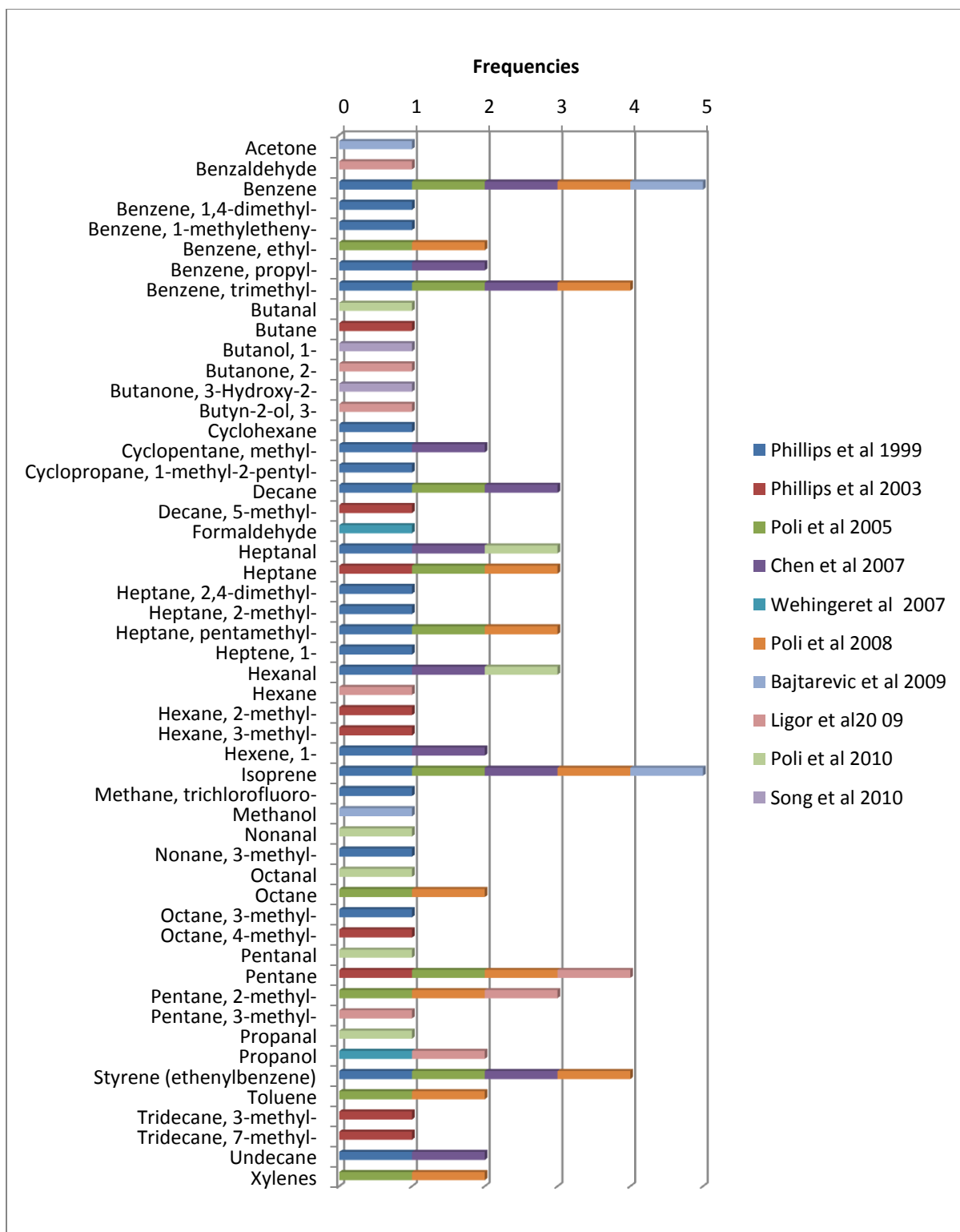


Figure 1 Examples of potential lung cancer-related breath biomarkers. Frequencies represent the number of papers citing each compound (27, 35-37, 39-45).

1.2.4 Current human breath analysis techniques

Various forms of breath analyzing techniques have been designed for different purposes: An alcohol breath analyzer is commonly used worldwide to deter operation of a motor vehicle by an impaired driver. It is purposely designed for blood alcohol level testing only and has no way to work for other types of exhaled substances. Electronic nose (46), is an interesting and cost-effective development. The semiconductors arrays can generate series of electronic signatures from the analyte but electronic nose has difficulty to give accurate quantifiable information to correlate VOCs. Interestingly enough, researchers have demonstrated breath analysis for lung cancer patients by trained dogs (47), but this approach may not be suitable for clinical settings. However, these non-spectroscopic methods for breath analysis do not give signals to specify analytes and therefore cannot be used for molecular identification purposes.

Spectroscopic breath analysis tools offer advantages for the identification and quantification of exhaled substances. There are two major types of spectroscopic methods for breath analysis, mass spectrometry and laser spectroscopy. Mass spectrometry has been widely accepted as a powerful analytical technique that measures the mass-to-charge (m/z) ratio of charged molecules, and it has a historical term called mass spectroscopy. Laser spectroscopy is a general term to describe analytical measurements based on the optical-medium interactions such as photon absorption and photon scattering using a laser source.

1.2.4.1 Mass spectrometry-related techniques for breath analysis

Mass spectrometry (MS) has long been playing an important role in various fields, such as food, medicine, forensic, sports, for the identification and quantification of unknown substances based on the analytes' m/z ratios. Most of the early findings in breath analysis were done with MS-based analytical tools. MS is generally sensitive enough for breath component analysis in trace amounts but some may require a pre-separation procedure to analyze individual compounds in a sample mixture of VOCs. Precursor ions for sample ionization are important to determine the versatility of the MS-based system. For the trace particles in expired breath to be detectable and truly quantified, there have been upgrades and other technologies combined with MS for performance enhancement, such as gas chromatography-MS (GC-MS) (27, 34), proton transfer reaction-MS (PTR-MS) (33, 48) and selected ion flow tube-MS (SIFT-MS) (49, 50).

Gas chromatography-mass spectrometry (GC-MS) is one of the most useful analytical techniques in breath analysis. Pre-separation procedures (such as GC) are usually indispensable to MS with enhanced analytical power for the analysis of complex gas mixtures. Gas chromatography (GC) is one of the most common pre-separation techniques combined with MS. GC separates molecules by their chemical properties in its capillary, resulting in different retention times. This results in molecules entering the downstream mass spectrometer separately and allows GC-MS to analyze complex mixtures of gases in a sequence. Molecules entering MS are then broken down into ionized fragments and analyzed according to their m/z ratios. This technique gives detailed information of the analyte but it generally requires sample pre-concentration to increase the sensitivity of the device.

The idea of using proton transfer reaction-mass spectrometer (PTR-MS) on real-time measurements of VOCs was introduced in the 1990s and has grown rapidly in usage since then (51). PTR-MS differs from traditional MS by sample ionization: H_3O^+ is used for ionization instead of the electron ionization. Sample gaseous molecules receive a proton from the donor (H_3O^+), thereby becoming ionized.

Selected ion flow tube-MS (SIFT-MS) is similar to PTR-MS but it makes use of more choices for the precursor ion for chemical ionization: H_3O^+ , NO^+ , or O_2^+ . It allows absolute quantification (49) and no sample pre-concentration is required for the modern SIFT-MS to achieve high sensitivity. The low fragmentation of analytes makes it easier for the analysis of complex molecules.

The various types of technique combined with MS are versatile and reliable. Techniques complement each other and each technique has their unique advantages and shortcomings: GC-MS has reliable molecule identification ability but suffers from the requirement of pre-concentration procedures and slow response time. PTR-MS works in on-line and with real-time breath sampling but fails to work for isobaric ions. SIFT-MS offers multiple precursor ions to work for molecules with the same m/z ratio but it has reduced sensitivity. Most MS-based breath analyses are undertaken in research laboratory settings. Although there are MS field units, they are specifically designed for certain types of target molecules for only limited use. Researchers and commercial companies have been attempting to reduce the size and cost. However, these are still intrinsic problems with MS which hinder its mobility and general applications.

1.2.4.2 Laser absorption spectrometry-related techniques for breath analysis

Laser absorption spectroscopy (LAS) techniques, which measure the photon absorption properties of an analyte, have been known for decades but have only become available for trace amount detection for breath analysis recently. Due to the fast development of semiconductor lasers and photodetectors, it has undergone recent advancements that enable high sensitivity and selectivity for real-time breath analysis for clinical uses (52-54). There are major laser spectroscopic techniques with sufficient sensitivity for breath analysis that have undergone increasing investigations over the past decade, including cavity ring down spectroscopy (CRDS) (55, 56), tunable diode laser absorption spectroscopy (TDLAS) (57, 58) and photoacoustic spectroscopy (PAS) (59).

Cavity ring down spectroscopy (CDRS) is a very sensitive optical device and can be used to monitor trace gas levels (60). It relies on long interaction pathways provided in the optical cavity by at least two highly reflective mirrors in specific wavelength. Photons bounce back and forth within the ultra-low-loss cavity and thus the effective optical interaction length can be increased more than 10,000-fold (54). Ring-down decay time is the measurement of photon leakage of the cavity in a particular frequency band to measure the sample concentration of a particular analyte. The ring-down time decays exponentially and is independent of laser intensity output instability. Absorption process can be shown by gradual decay of the laser intensity and hence the concentration of the sample gas.

Tunable diode laser absorption spectroscopy (TDLAS) is a combination of the traditional laser absorption techniques with tunable diode lasers, which measure the absorption

characteristics of the sample molecules by scanning across its particular central absorption peak. TDLAS can give not only sample concentration information but also the temperature and pressure of the gas analyte. TDLAS can be integrated with a Herriott cell (multipass) consisting of concave mirrors. The laser beam comes out of the cavity at a different angle than the incoming beam, unlike the high finesse optical cavity of CRDS. Its effective beam path is considerably shorter than CRDS, but the Herriott cell can still lengthen the effective absorption path by 10- to 100-fold and offers a limit of detection in the order of 10^1 pptv (54).

Photoacoustic Spectroscopy (PAS) (59) is a spectroscopic technology based on indirect measurement of photon-molecule resonance (which converts light energy into sound energy). The setup usually involves microphones to detect sound waves produced during photon absorption by molecules. Therefore, the laser beam is not directly measured and the background is relatively weaker compared to conventional laser-based spectroscopy.

Each laser-based technique has its own advantages and limitations, and they complement each other. CRDS is precise and reliable, but it is untunable and limited in a narrow frequency range. Moreover, it requires an expensive narrow bandwidth laser and highly reflective mirrors for particular molecules; TDLAS is tunable and offers the possibility to access different frequency ranges in the mid-IR region, but the cost of a tunable diode laser is still the main consideration; PAS employs indirect acoustic measurements to avoid major laser background noise, but the noise issue is still challenging for such weak photoacoustic conversion. Failure or difficulty with multiplexing is one of the biggest challenges for LAS-

based breath analysis since one disease/disorder can contain multiple biomarkers that have well separated absorption lines. With the advent of laser diodes and photoelectronics, different new techniques integrated LAS-based breath analyzers with better functionality and lower cost with may have an important role in the future.

1.3 Raman scattering and fibre optics

1.3.1 Raman scattering

The Raman effect is named after the Indian Physicist Chandrasekhara V. Raman for his discovery of this radiation effect in 1928 (61). When photons interact with atoms or molecules, most photons scatter elastically. This process is called Rayleigh scattering in which there is no net energy transferred to the molecule by the incident photon. In other words, the molecule is excited to a virtual state by the incident photon with frequency ν_0 and then re-emits a photon with the same frequency ν_0 . On the other hand, photons can be scattered inelastically so that the outgoing photon may have more or less energy than the incident photon due to energy transfer. Raman scattering is one kind of the inelastic process that causes change in energy of photon due to the molecular motion (62). Almost all of the photon-molecule interactions undergo Rayleigh scattering, only about 1 in 10^6 of photon-molecule interactions result in Raman scattering (63).

Raman scattering depends on molecular vibrations. For example, there are many different molecular vibrations of a triatomic molecule, including the symmetrical and anti-symmetrical stretching, scissoring, rocking, wagging and twisting motions (64). Molecular vibrational

modes are unique features of every molecular species and this offers the ability of Raman spectroscopy to provide fingerprint-type spectra for molecular identification.

For a molecule excited from the ground state by a photon, a new photon can be re-emitted with frequency $\nu_o - \nu_m$, where ν_m is the vibrational energy of the Raman-active mode of the molecule. In this case, a portion of the optical energy from the photon is transferred to the kinetic energy of the molecule and this red shift in wavelength is called Stokes Raman scattering. If the photon is scattered by a molecule in a vibrational state, the photon energy and vibrational energy can be released in terms of a single photon with frequency $\nu_o + \nu_m$. In this case, the kinetic energy of the molecule is transferred to the optical energy of the Raman-scattered photon. This blue shift in wavelength is called anti-Stokes Raman scattering, as illustrated in Figure 2.

In simple terms, processes involving an excited photon returning to the original, higher or lower vibrational levels are called Rayleigh, Stokes Raman or anti-Stokes Raman respectively. Note that the intensity of the anti-Stokes Raman lines should normally be weaker than the Stokes lines because there is a smaller population of molecules in a higher energy level, therefore, less photon-molecule interactions originate from a vibrational excited state.

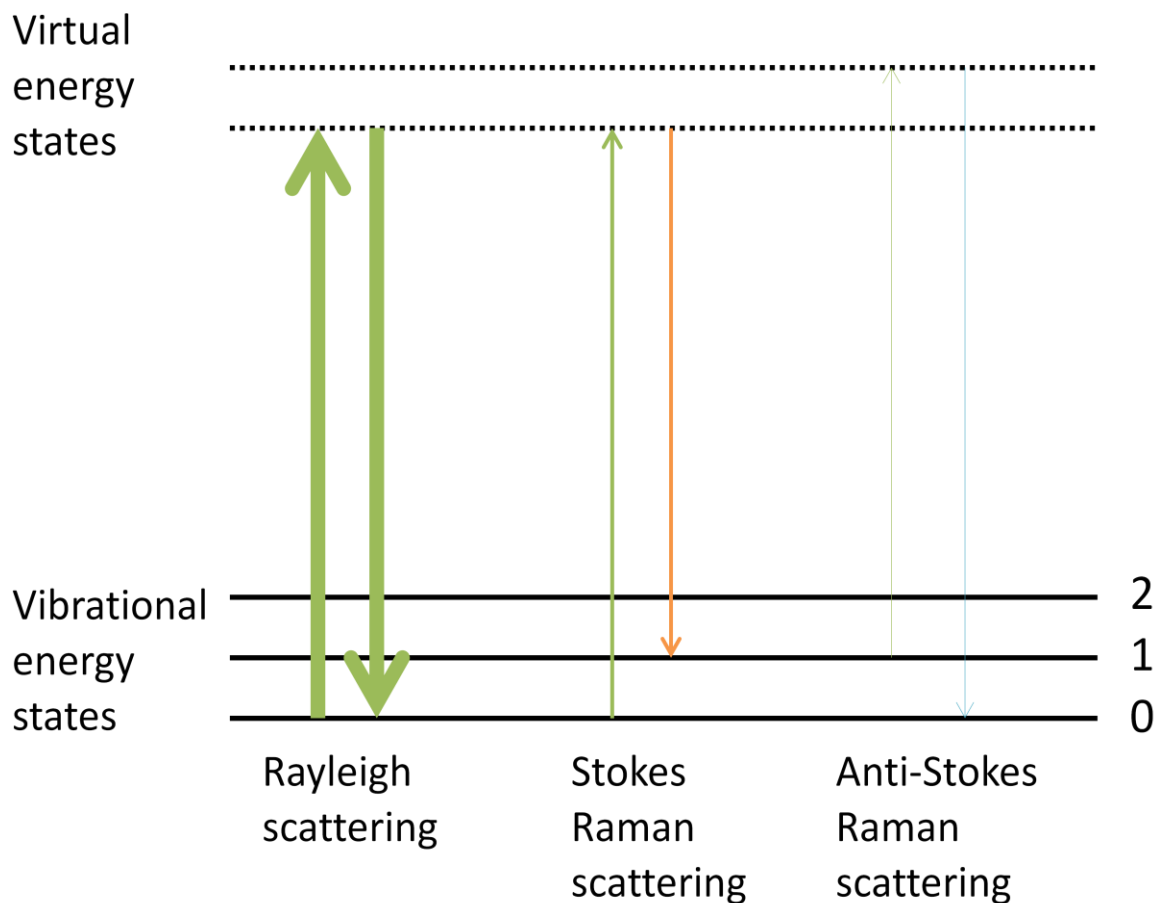


Figure 2 Energy level transitional schemes showing Rayleigh scattering, Stokes scattering and anti-Stokes scattering. 0, 1, 2... are the ground state and subsequent vibrational states of the molecule.

A typical Raman system should be pumped by a laser for excitation in the region from UV to near-Infrared. The Raman shifted emissions can be measured with an optical system and a spectrometer. Raman shifts are conventionally measured in relative wavenumber in the unit of cm^{-1} . Wavenumber is a property of a wave expressed in the inverse of wavelength, i.e., directly proportional to energy. Relative wavenumber is a representation of the difference between the wavenumbers of the excitation light and the Raman-scattered photon, which is directly proportional to the energy gap of the vibrational level to the ground state of the molecule.

1.3.2 Fibre optics

1.3.2.1 Conventional optical fibres

Optical fibres are light guides that direct light from one end to the other end of the fibre. Fibre optics has been extensively used in medical devices as light guides, in computer networking and in telecommunications. Conventional optical fibres are usually composed of a solid silica core for light transmission, cladding to provide difference in optical density and jacket for protection, as shown in Figure 3. Bare fibres for commercial application are not common but usually terminated with standard connectorizations.

The core and cladding of the fibre are made of materials with different refractive indexes, such that light is guided by the principle of total internal reflection. Optical fibres that make use of this working principle are called index-guiding fibres. If the incident light travels from an optically denser medium to a less dense medium with an angle greater than the critical angle, light should be reflected obeying the law of reflection. Equation 1 shows the relation between the refractive indexes and the maximum acceptance angle θ_{\max} , where n , n_1 and n_2 are the refractive indexes of the propagation medium (1.0 for air), the core and cladding of the fibre respectively.

$$NA = n \sin \theta_{\max} = \sqrt{n_1^2 - n_2^2} \quad (1)$$

To satisfy the condition of total internal reflection, the refractive indexes n_1 has to be greater than n_2 . In this case, light propagates in the silica core with low loss of refracted light escaping the fibre. Light rays with incident angles greater than θ_{\max} would probably not propagate through the fibre and are most likely absorbed by the fibre jacket. The acceptance cone is a geometrical description of the acceptable light rays which are coupled into the core

of the fibre with the largest incident angle, which has a calculated value called numerical aperture (NA). In conventional index-guiding fibres, light is always confined in the solid core but has low chance to interact with gas molecules around the fibre, and thus is not effective for gas sensing.

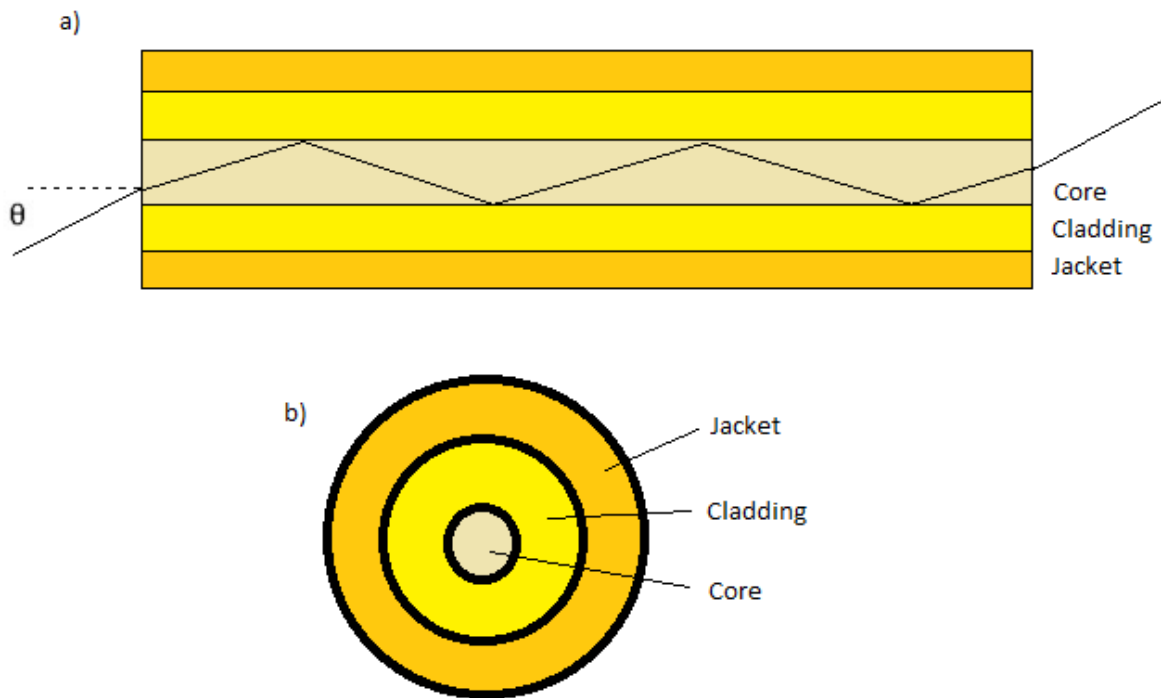


Figure 3 Illustration of a) light ray transmission in the fibre core, b) cross-sectional structure of an optical fibre.

1.3.2.2 Photonic crystal fibres (PCF)

Photonic crystal fibres (PCF) are a new technology of light guides which can confine light in a small volume by making use of a periodic microstructure made of silica. The most common technique to fabricate PCFs is called stack-and-draw; silica capillaries can be stacked up, fused together and drawn down to form the PCF (65). There are mainly two types of PCFs, solid core and hollow core with microstructured holey cladding. The index-guiding principle

can hold for solid core PCF with photonic crystal cladding. On the other hand, conditions for total internal reflection cannot be satisfied for hollow core-PCF (HC-PCF). HC-PCF has another name, hollow core-photonics band-gap fibre, because it guides light by its unique honeycomb-like microstructure and is only highly reflective on certain wavelength ranges as a result of multiple constructive interference from Bragg reflections. The microstructured photonic band-gap cladding (two-dimensional photonic crystal) is carefully engineered so that it forms high and low refractive indexes periodically. The geometry and the air filling fraction of photonic crystal cladding are keys to determine the band-gap guidance properties, therefore different cladding structures can result in different transmission bands (66). Certain wavelengths would experience very high scattering effect in the cladding region because the Maxwell's equations do not provide propagation solution for the wavelengths out of the band-gap region (67). So the wall of the core acts as a highly reflective surface to photons with these particular wavelengths and guides light through the fibre obeying the law of reflection. The hollow core of HC-PCF is gas-fillable with gas molecules so the fibre can be treated as a tiny hollow tube.

1.3.3 Raman scattering in HC-PCF

Spontaneous Raman scattering is a multi-directional process and the conversion efficiency is low in general. Focusing a laser beam to a focused spot would increase the power density of the laser and thus enhance the number of photon-molecule interactions in a small volume. Figure 4a shows a free space setup with a converging lens to focus the laser beam to a small focused spot. This free space setting has a small interaction volume and is inefficient for Raman-scattered photon collection as the signal is unguided. Therefore, most of the signals

are lost and cannot reach the detector properly. Furthermore, filters are hard to set up in this configuration to get rid of the detector saturation problem caused by the laser photons. Figure 4b shows a laser beam focused to a hollow capillary fibre with an internal reflective coating. This type of hollow capillary fibre can be filled with liquid or gas sample and allow Raman signal to be generated and guided in the hollow core. However, this type of capillary normally has strong leakage of the coupled light and the NA of the capillary is usually low. Therefore, the generation and collection efficiencies of the Raman-scattered photon are still low. A research group in Japan has tried using this type of capillary fibre for gas analysis and achieved detection limit of about 2000 ppmv of oxygen gas in air (68). Figure 4c shows our proposal of using HC-PCF to replace hollow capillary fibre to enhance Raman scattering in the core of the fibre. HC-PCF has low-loss band-gap guidance for laser photons if the laser beam is properly coupled. HC-PCF can offer typical NA values and can be coiled up to few centimeters in radius with no significant drop in the transmission. The HC-PCF serves as a hollow tube in which the core can be filled with gaseous Raman-active samples. HC-PCF offers a perfect place for photon-gas molecule interaction as the coupled light and gas molecules can be confined in the focused volume. The tight confinement provided by the core of HC-PCF hugely increases the number of photon-molecule interactions, which significantly enhances the Raman scattering signal of the specimen. The guided Raman signal can then be collected easily with typical optics settings and analyzed with a Raman spectrograph.

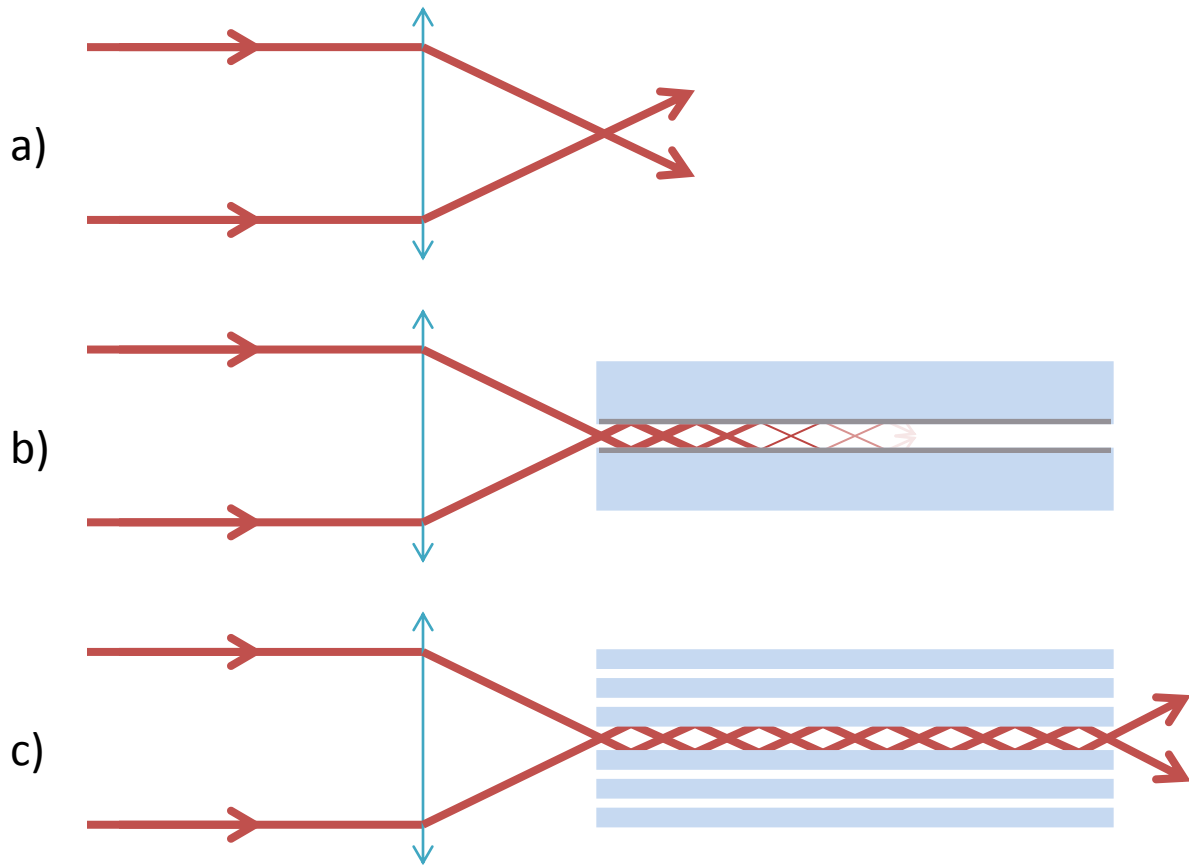


Figure 4 Comparison of a laser beam a) focused to free space (no light guide); b) focused to a high attenuation hollow tube with inner reflective coating (thickness of the arrows represent the intensity of the light rays); c) focused to a low attenuation HC-PCF.

1.4 Hypothesis and objective

Lung cancer is the leading cause of cancer death in Canada according to the Canadian Cancer Society (69). One of the main reasons for this is because lung cancer cases are usually diagnosed in an advanced stage. There is a higher chance of metastases and complications in advanced stage lung cancer resulting in low survival rates. Currently, there is no lung cancer screening tool generally accepted by health professions as these tools are usually inefficient and considered invasive and, as a result, not effectively benefiting the public. There has been

an overwhelming need to have a simple, non-invasive and cost-effective lung cancer screening tool for frontline medical uses.

Breath analysis has long history in the medical field and has the capability to offer useful information in cancer screening since substances contained in exhaled breath are unique and different for everyone based on the state of the human body. Most of the early findings of breath analysis were done by mass spectrometry, or more recently with laser absorption spectroscopy. Studies based on these spectroscopic techniques have shown that breath analysis is able to show different results between lung cancer patients from healthy controls. However, these techniques may not be easily applicable to clinical settings as they are usually expensive and large in size.

Raman spectroscopy is a promising candidate for breath analysis because of its ability of molecular identification. Raman scattering is one kind of photon-molecule interaction, photons interact with molecules causing excitation and de-excitation, which generate fingerprint-type spectra due to the unique molecular kinetic modes of the analyte. However, the efficiency of Raman scattering is low and the unguided signals in free space are weak. Photonic Crystal Fibre (PCF) is new technology in fibre optics that allows light to travel through a hollow core with low transmission loss by band-gap guidance. The hollow core of PCF can be filled with gas phase samples and thus confine photons and Raman active media in a small space to enhance Raman signal strength. Spectroscopic information can be obtained from the breath-filled PCF to perform molecular identification. Therefore, the

Raman spectral analysis of the exhaled breath samples from lung cancer patients and healthy controls may give clues to develop a lung cancer screening tool.

Our goal is to develop a simple, cost-effective and non-invasive tool based on Raman spectroscopy for breath analysis and potentially lung cancer screening. In this project, the plan is to develop a prototype of a Raman-gas cell based on HC-PCF for spectral analysis. Second, the performance of this Raman-gas analyzer based on the spectroscopic signals obtained from reference gases and human breath sample is investigated. Third, the detection limit of this Raman-gas analyzer is compared with a recent publication based on hollow capillary fibre (70). The plausibility of detecting lung cancer-related exhaled biomarkers based on the detection limit of the prototype is investigated.

Chapter 2: System development

In this chapter, the design and construction of the Raman cell based breath analyzer prototype are described. The Raman-gas cell system contains mainly two parts: photonics - the optical system provides laser illumination and the collection of the Raman signals for spectroscopic analysis; and the gas filling system - the tubing and fitting system provides pressure difference in a closed space for gas loading and unloading to the HC-PCF.

2.1 System overview

Figure 5 shows a schematic diagram of the entire Raman-gas cell system. The 785 nm single mode continuous wave (CW) laser (I0785SA0100B, Innovative Photonic Solutions), 100 mW max power and 1 MHz linewidth, is used as an excitation pump source. The laser beam passes through a reversed 5x beam-expander (NT59-135, Edmund Optics) with near-infrared coating to shrink the diverse beam from around 10 mm down to 2 mm. The laser beam is then focused by an aspheric lens with 18.4 mm focal length (C280TME-A, Thorlabs) to the core of the HC-PCF (HC-800-01, NKT Photonics). The HC-PCF is held by a vacuum fibre optics feedthrough (VACUUM-01-T-0.125, OZOptics) connected to the tubing system through the in-house customized gas chamber fitting. The gas chamber is attached to a precise series xyz-fibre alignment stage (ULTRAlign 561D, Newport) for coupling alignment. The emission end of the ~ 2.5 m long HC-PCF is held by a similar configuration as the illumination end. The emission cone, containing the laser and Raman-scattered signal, is collimated by an aspheric lens with a 13.86 mm focal length (C560TME-A, Thorlabs). The collimated beam passes through a long pass filter (LP01-785UR, Semrock) to block the laser beam and release the Stokes Raman signals. The filtered beam is then refocused by an

aspheric lens with 15.29 mm focal length (C260TME-A, Thorlabs) onto a 50 μm multimode SMA-connectorized fibre (M14L01, Thorlabs). The 50 μm fibre guides the signal to a spectrograph (HoloSpecTM $f/1.8$ Spectrograph, Kaiser Optical Systems) for spectral separation. A 100x1340 pixel, liquid nitrogen-cooled, back-illuminated, deep depletion, near-IR optimized, CCD camera (Acton 7508-0002, Princeton Instruments) was used to capture the Raman spectra from the spectrograph. Liquid nitrogen cooling to low temperature of the CCD allows long integration of the Raman signal to increase the signal-to-noise (S/N) ratio. With the 50 μm multimode signal collection fibre, according to the users' manual, the spectral resolution of the spectrometer for the low-frequency Stokes grating (HSG-785-LF, Kaiser Optical Systems) is around 4 cm^{-1} .

It is worth noting that a combined forward- and back-scattered mode, with a short pass dichroic filter and linear fibre array adapter, was tested but it showed no significant improvement in the signal-to-noise ratios. The explanation and possible improvements of this optical configuration are discussed in section 4.1 and 4.2.

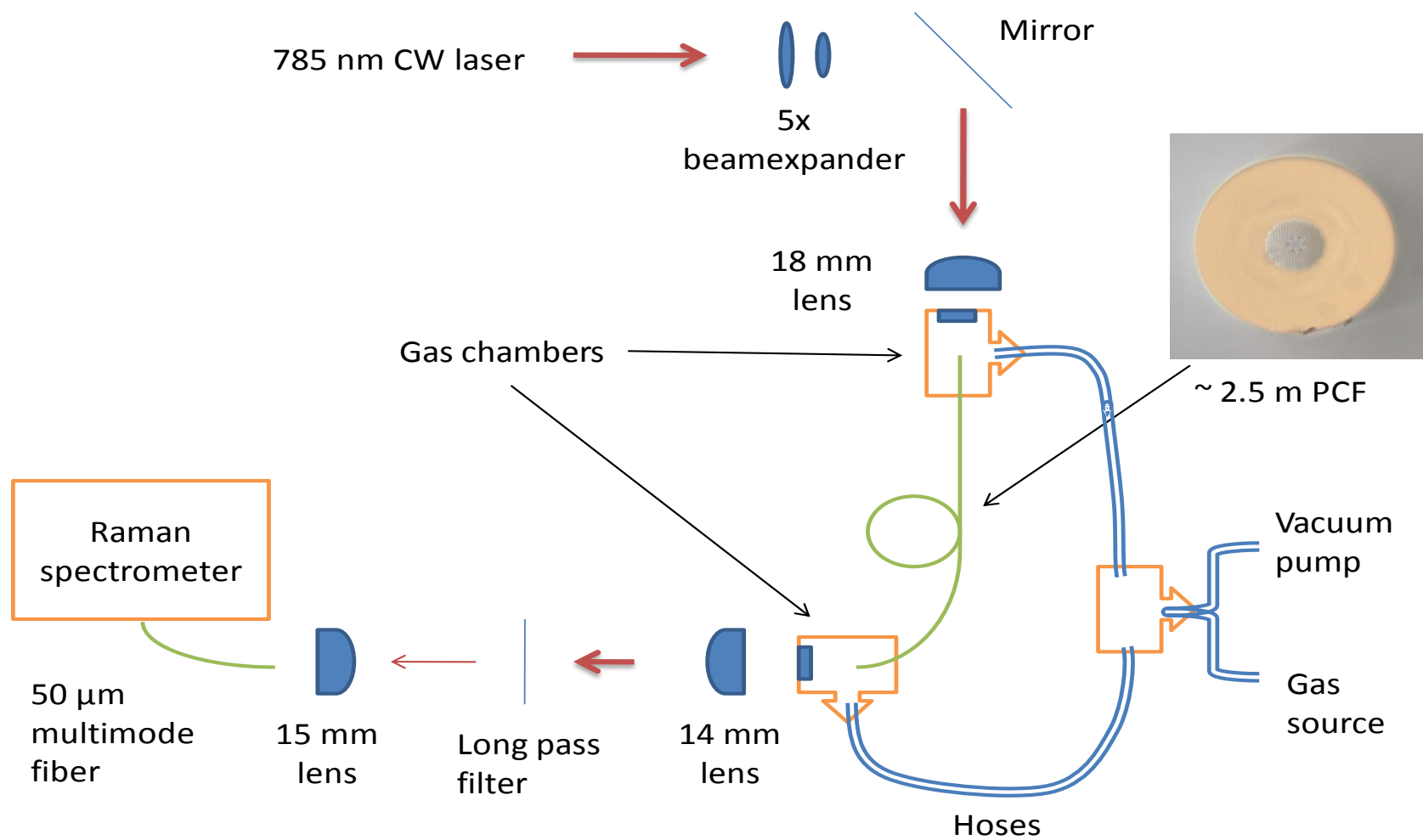


Figure 5 Schematic diagram of the Raman-gas cell system.

2.2 HC-PCF

The fibre used in this project was a photonic crystal fibre with a hollow core (HC-800-01). This fibre is made of silica and the holey region is made with unit cells (hollow capillaries). The hollow core was made by removing the 7 unit cells in the middle of the photonic crystal (PC) cladding. The core is hollow through the entire fibre so that it can be filled with gas by suction. Raman signals generated in the hollow core of the HC-PCF can be guided through the optical components and collected by a Raman spectrometer for analysis.

The usable laser and Raman-signal range are limited by the band-gap guidance range of the fibre, which is governed by the attenuation curve of the fibre. Approximately, a wavelength range from 780 nm to 880 nm would experience transmission losses of less than 350 dB/km (equivalent to around 8% power loss per meter). This fibre is commercially available from NKT Photonics and the fibre specification is as follows:

Core diameter	10 μm
Holey region (PC cladding)	40 μm
Solid cladding diameter	135 μm
Outer coating	220 μm
Centre wavelength	830 nm
Attenuation (780-880 nm)	<350 dB/km
Mode field diameter (x-,y-average)*	8.8 μm

Table 1 Specifications of the HC-800-01 HC-PCF (sourced from the manufacturer's datasheet)

**The mode field diameter of the core is measured by the average of x-and y- near field intensity of the fibre output profile.*

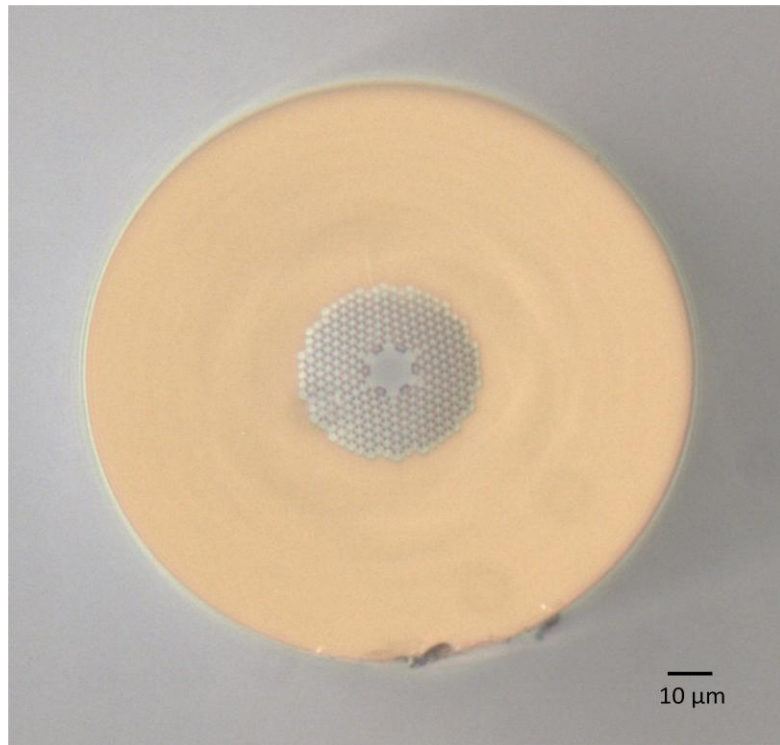


Figure 6 Cross-sectional view of HC-800-01 under a 20x microscope objective.

Figure 6 shows a cross-sectional image of the tip of the cleaved HC-800-01 taken with a 20x objective lens and camera in our laboratory. The image shows a star-like core (10 μm) in the centre of the fibre, the honeycomb-like microstructured region (40 μm), and the traditional silica cladding (135 μm). The outer coating was stripped off by a fibre stripper (CFS-2, Clauss). The fibre coating should be removed for at least 1 cm for the tip to be properly cleaved by the fibre cleaver (CT-30, Fujikura). It is worth noting that less than 5 mm of the fibre coating should be stripped off each pass to prevent breakage of the fibre, meaning that the coating should be removed in at least two passes. The cut tip can be carefully glued and aligned vertically on a microscope slide to check the cleaving quality under a microscope. Poor cleaving quality can lead to unsatisfactory laser beam coupling efficiency. The cleaved PCF tip should not be cleaned by any cleaning agent because the holey region may easily be

filled with any liquid by the capillary effect. It is also important not to touch the fibre tip throughout the experiment because dirt can attach on the fibre tip and absorb laser energy, leading to poor laser coupling or even damage to the fibre tip. Therefore, the fibre should be inserted into the vacuum fibre optics feedthrough before cleaving to avoid leaving any dirt on the tip during the process.

2.3 Gas chamber and tubing system

The HC-PCF can provide laser guidance and at the same time be gas-fillable. This hollow fibre can be treated as a hollow tube-cell with 10 μm diameter. Pressurized or atmospheric pressure gas samples can be pumped through the hollow core of the HC-PCF integrated with the gas chamber and tubing system. In order to provide a sealed environment for the gas cell, gas chambers are needed on both ends of the fibre without blocking the transmission of light. Apertured and sealed gas chambers are therefore designed to serve this need. It is mainly composed of two parts, the fibre optics feedthrough and customized gas fitting. The fibre optics feedthrough is to hold the fibre into position and it is sealed by tightening a plastic sealant. The fitting is 90 degree street elbow 1/8" with NPT thread made of brass. A 2-step hole was drilled with two different drill heads (6.4 mm and 3 mm) to support the sapphire window and provide an aperture for light transmission. Figure 7 shows the schematic diagram of the gas chamber design. The sealed feedthrough is connected to one end of the apertured fitting by 1/8" NPT thread. The sapphire window (SAW12, Newport), 6.35 mm in diameter and 0.5 mm thick, is sealed and glued onto the brass fitting by silicone sealant. Sapphire windows are ideal for applications where high pressure, vacuum, or corrosive atmospheres are considerations. The threshold pressure of this sapphire window is ~ 1600 psi

but the highest pressure tested on this configuration was ~ 250 psi, which is the limit of the reference gas regulators. The other end of the brass fitting is attached to a push-to-connect tube fitting with 1/8" NPT thread. Both ends of the fibre have the same gas chamber setting and are connected by the plastic tube through the push-to-connect fittings. The tubes are connected to a vacuum pump and the gas source for gas unloading and loading by pressure difference. Not shown in

Figure 5, pressure gauges are used to monitor the filling process and internal pressure; ball valves are employed to control the gas flow and discharge process. All fittings, valves and pressure gauges are connected by the 1/8" outer-diameter plastic tubes.

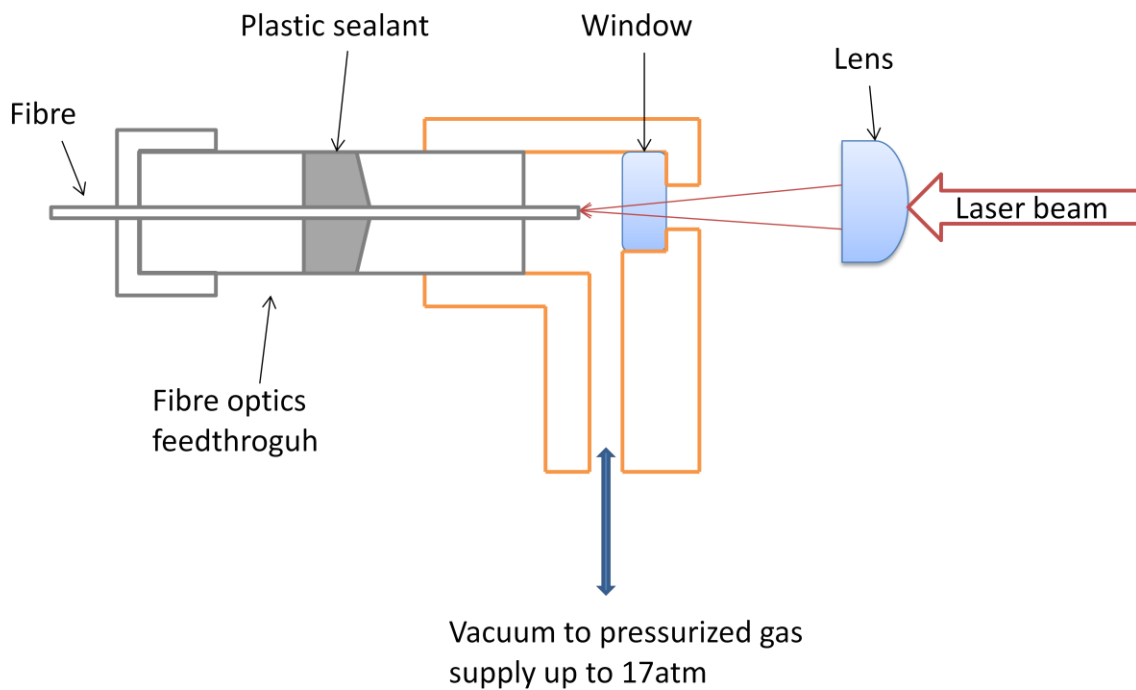


Figure 7 Schematic diagram of the gas chamber design.

The incoming laser beam can be focused by an aspheric lens and the laser cone hits the sapphire window attached on the custom brass gas fitting then reaches the HC-PCF. To couple the laser into the core of the fibre, the whole gas chamber was bolted down and aligned by a xyz-translation stage. Fibre coupling can be achieved by maximizing the coupled laser power monitored by a laser powermeter on the emission end. To achieve the best laser coupling, the fibre portion sticking out of the feedthrough should be kept in an optimal position such that it is as close as possible to the sapphire window but not in contact. Otherwise, the optical guidance and gas filling process can both be affected.

Chapter 3: Results and analysis

In this chapter, several reference gas samples (oxygen gas, hydrogen gas, carbon dioxide gas) obtained from Praxair were tested to verify the calibration and response of the system; human breath was tested to identify some major exhaled components; ambient air was tested to find out the limit of detection of this prototype.

3.1 The measurements of reference gases

3.1.1 The measurement of oxygen gas

A tank of pure oxygen gas was connected to a CGA-540 gas regulator with the maximum safety working pressure 250 psi. The oxygen gas Raman spectrum in this spectral region contains a vibrational line at 1556 cm^{-1} with 1.2 differential Raman cross-sections (71). The fine structures on both sides of the central vibrational peak are the rotational lines (72). In our experiment, a sharp peak was observed at 1557 cm^{-1} , along with peaks with lower intensities and symmetrical pattern extending 150 cm^{-1} from both sides of the sharp peak, shown in Figure 8. Zooming into the fine structure, the rotational lines were almost evenly spaced $\sim 12\text{ cm}^{-1}$ apart, the intensities of the lines were maximum at $\sim 50\text{ cm}^{-1}$ away on both sides from the central vibrational peak. This measurement was taken in 0.3s exposure time with 200 psi gas pressure.

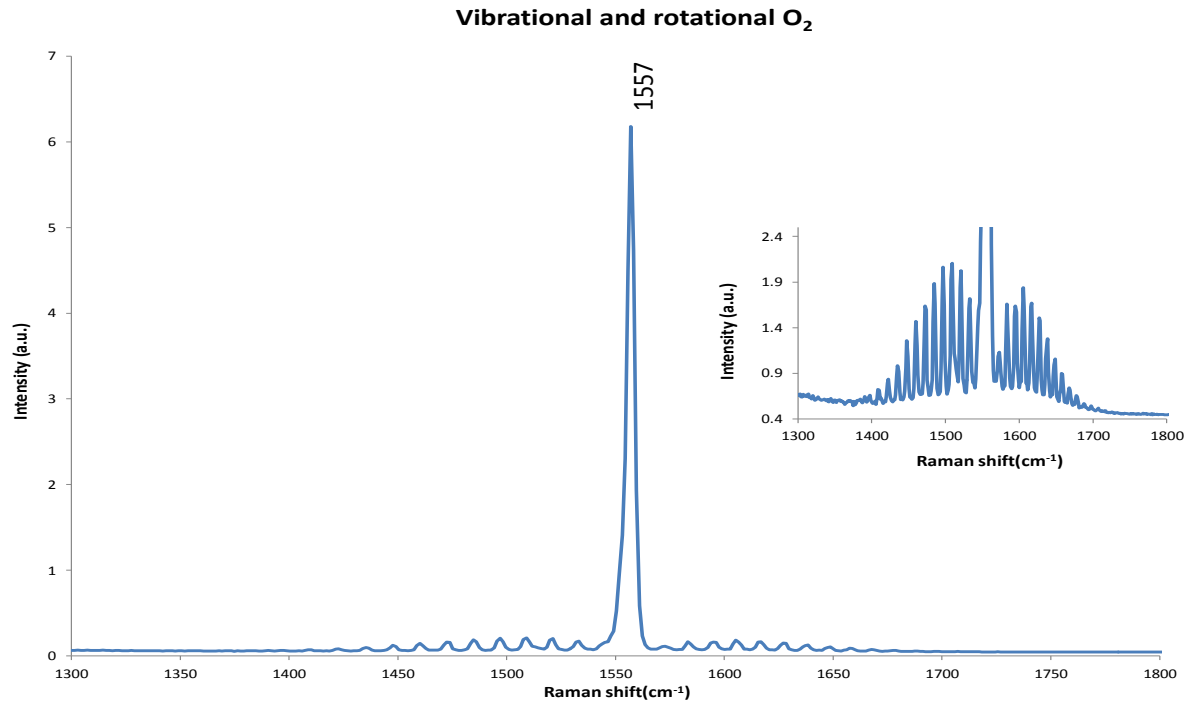


Figure 8 The measured vibrational and rotational spectrum of the pure oxygen gas by the Raman cell.

3.1.2 The measurement of hydrogen gas

A tank of pure hydrogen gas was connected to the tubing system by a CGA-350 gas regulator with the maximum safety working pressure 125 psi. The published Raman spectrum of the hydrogen gas has four rotational lines within the spectral region of our spectrometer (73). The four lines observed in this experiment were at 584 cm⁻¹, 814 cm⁻¹, 1034 cm⁻¹ and 352 cm⁻¹ in decreasing order of the peak intensities, shown in Figure 9. The vibrational line of hydrogen gas at 4161 cm⁻¹ is out of the transmission band of the fibre and the spectral range of the spectrometer, therefore it is not observed. The other broad peaks and bumps in this spectrum are due to the Raman characteristic of the fused silica originated from the fibre materials. The measurement was taken in 1s exposure time with 100 psi gas pressure.

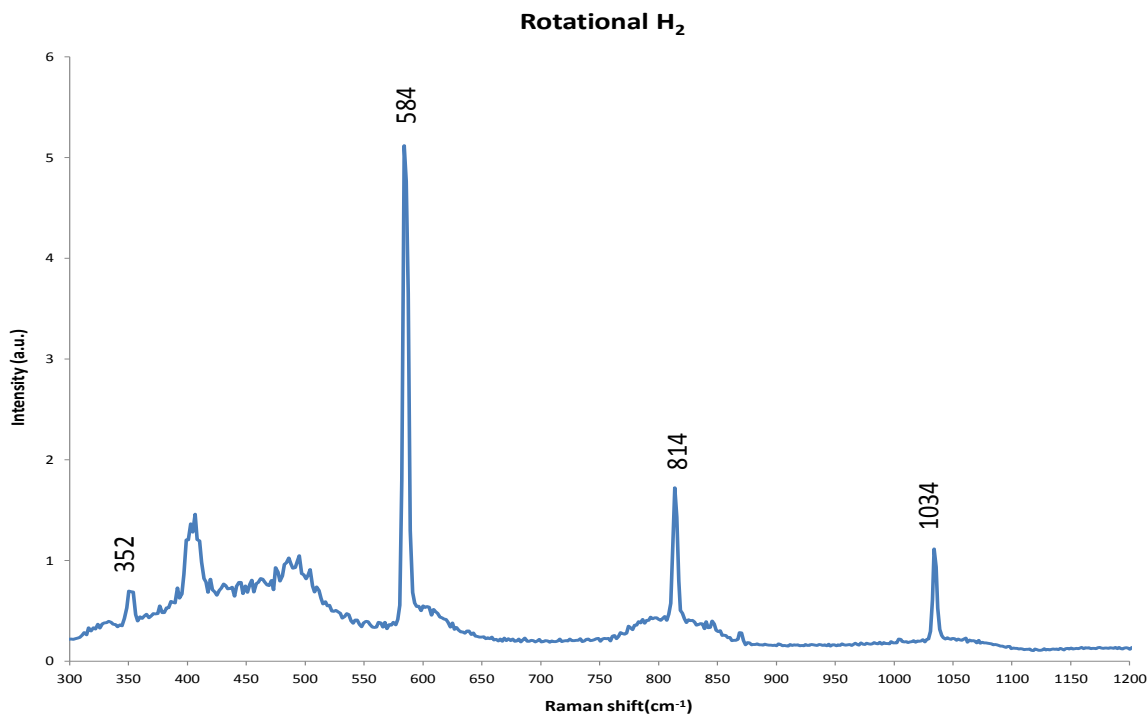


Figure 9 The measured rotational Raman spectrum of the pure hydrogen gas by the Raman cell.

3.1.3 The measurement of carbon dioxide gas

This tank contains 5% carbon dioxide gas in nitrogen gas. The outlet of the CGA-500 regulator was connected to the tubing system to supply this gas sample for analysis. The pressure of the gas was set to near atmospheric pressure such that it was close to the condition of human exhaled breath. The Raman spectral feature of carbon dioxide gas has two vibrational lines within the fingerprint region, at 1286 cm⁻¹ and 1388 cm⁻¹ with Raman cross-sections 0.89 and 1.4 respectively and generating the intensity ratio 0.64 (71). The two lines observed in this experiment were at 1286 cm⁻¹ and 1388 cm⁻¹ in increasing order of the peak intensities, shown in Figure 10. The intensity ratio measured in this experiment was around 0.61. The nitrogen gas peak is outside the spectral region of the spectrometer and therefore not observed. This measurement was taken in a total exposure time of 10 s.

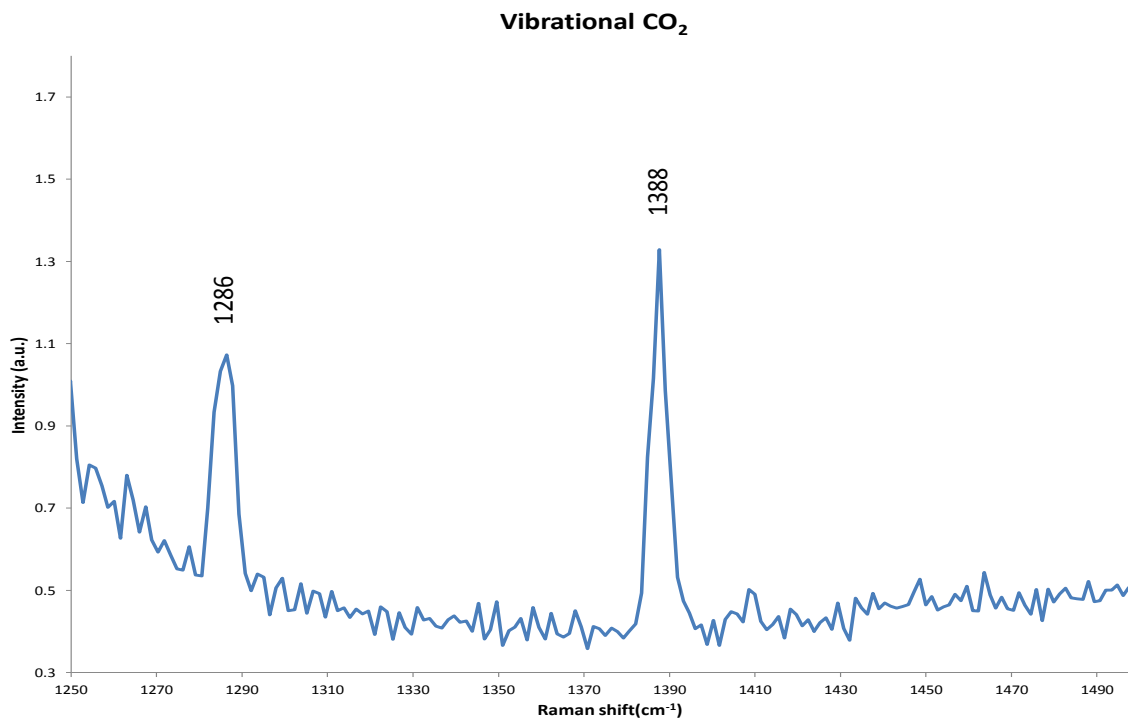


Figure 10 The measured vibrational Raman spectrum of the carbon dioxide gas by the Raman cell

3.2 The measurements of breath and ambient air

3.2.1 The measurement of human exhaled breath

Human exhaled breath was sampled by a collection bag with a sealed, one-way valve fitting connected to the tubing system under the ambient condition. In the low-frequency Stokes range, the Raman features of oxygen gas are 1556 cm^{-1} line and the rotational signatures; lines at 1286 cm^{-1} and 1388 cm^{-1} are the Raman features of carbon dioxide gas, shown in Figure 11. However, the nitrogen line at 2331 cm^{-1} and water vapour line at 3652 cm^{-1} cannot be observed in this optical configuration, because those lines are out of the spectral range of this spectrometer. The human breath exhaled O₂ (eO₂) and exhaled CO₂ (eCO₂) concentration are roughly 16% and 4% respectively, generating the ratio of eO₂:eCO₂ to be ~ 4:1. By the Raman cross-sections of the analytes (71) and peak ratios of this particular breath sample spectrum, the experimental estimation of eO₂:eCO₂ was found to be ~ 3.85:1. This

measurement was taken under room pressure with 23 s exposure time to the Raman spectrometer.

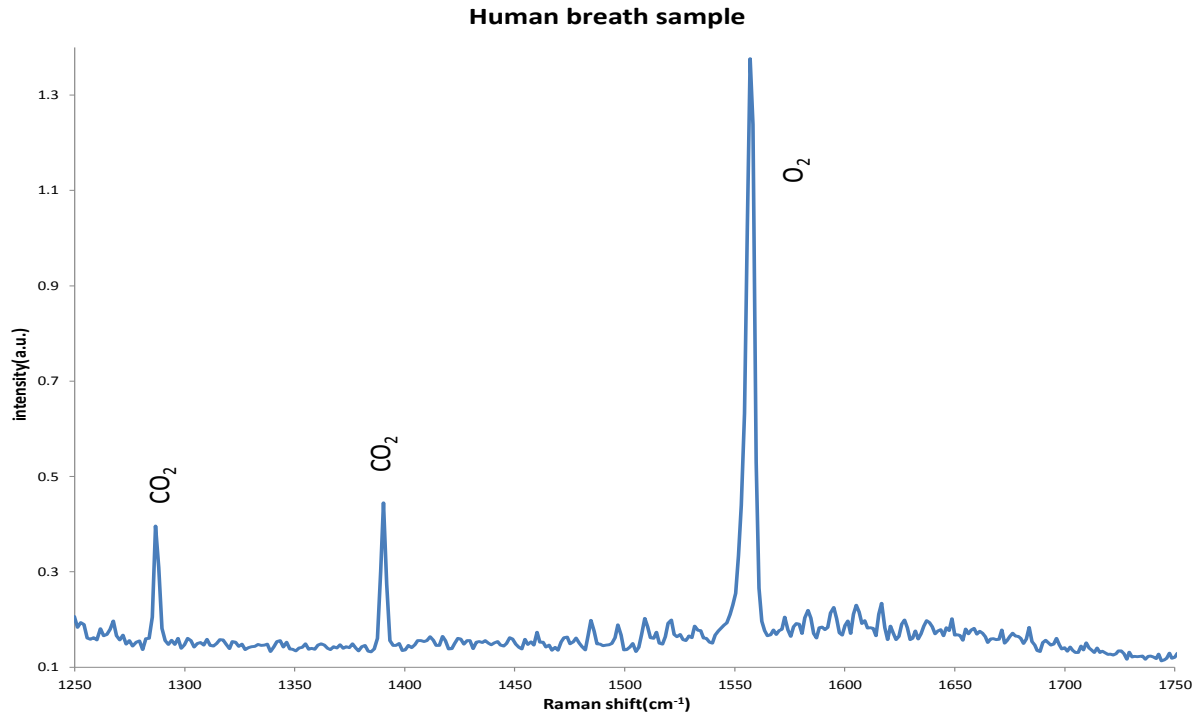


Figure 11 The measured human exhaled breath spectrum by the Raman cell showing Raman features of the carbon dioxide and oxygen molecules.

3.2.2 The measurements of the ambient air

The filling process of the ambient air is done by having the two ends of the fibre tip exposed to the air. Typical ambient air contains approximately 21% oxygen and 0.03% carbon dioxide gas. This measurement was taken in 5 s exposure time. The Raman features of the oxygen molecules, 1556 cm⁻¹ line and the rotational signatures are observed, shown in Figure 12. However, in this experimental condition, the carbon dioxide gas Raman features are not clearly observed. It is attributed to the low concentration level of the carbon dioxide gas in the ambient air. The weak Raman signals are obscured by the measurable background noise.

To reveal the overtaken Raman signals originated from low concentration molecules, it is recommended to improve the spectral signal-to-noise ratio, for example, by increasing the spectral integration time and measurement accumulation.

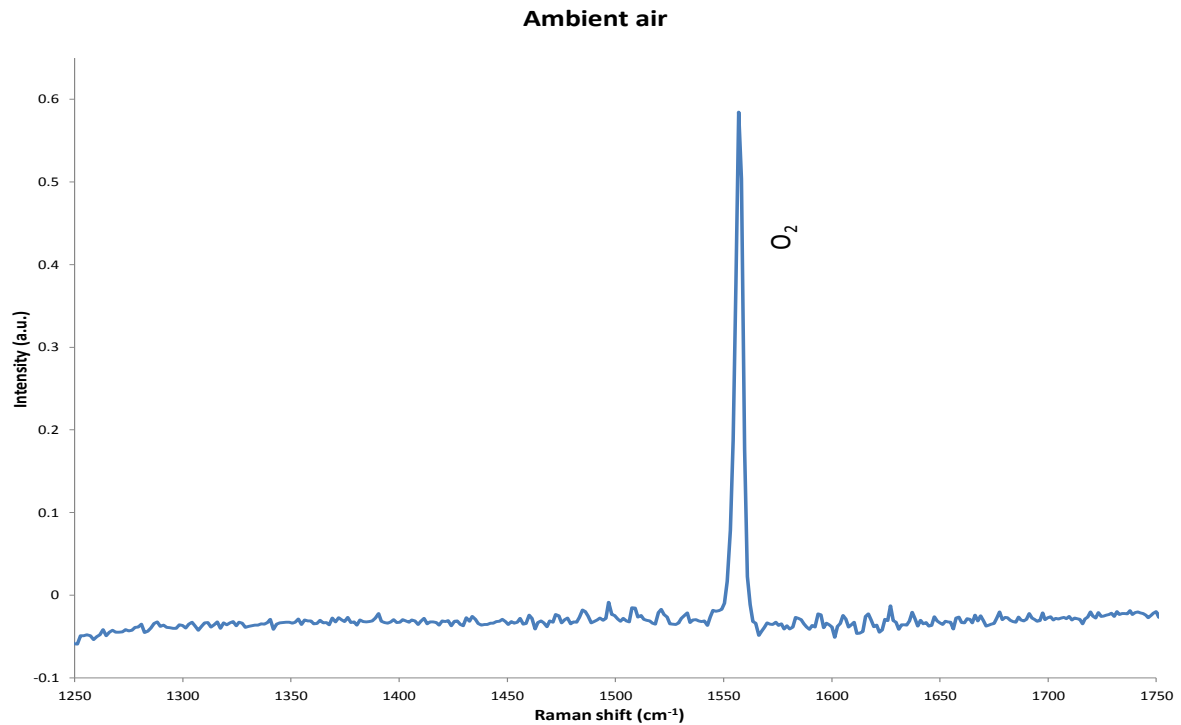


Figure 12 The measured spectrum of the ambient air by the Raman cell showing the Raman features of the oxygen gas

The experiment was done again to measure the concentration of carbon dioxide gas in the ambient air. It was carried out with longer exposure time (25 s) to reduce the readout noise of the detector and more repetition (150) to produce spectrum with the averaged statistical noise, shown in Figure 13. In this spectrum, the carbon dioxide vibrational Raman features and rotational oxygen Raman signatures extending to the shorter wavelength region were observed although the background was relatively noisy. The vacuum spectrum was subtracted to eliminate the Raman noise generated in the fibre, to reduce the background and

emphasize the targeted peaks. The vacuum spectrum was measured under the same optical configuration, but with the tubing system evacuated by the vacuum pump to remove particles in the core of the HC-PCF. However, the vacuum pump can only evacuate roughly two-thirds of the molecule population in the tubing system. Therefore, the signal intensity of carbon dioxide peaks in the background subtracted spectrum would only represent roughly 70% of the ambient concentration of the carbon dioxide molecules.

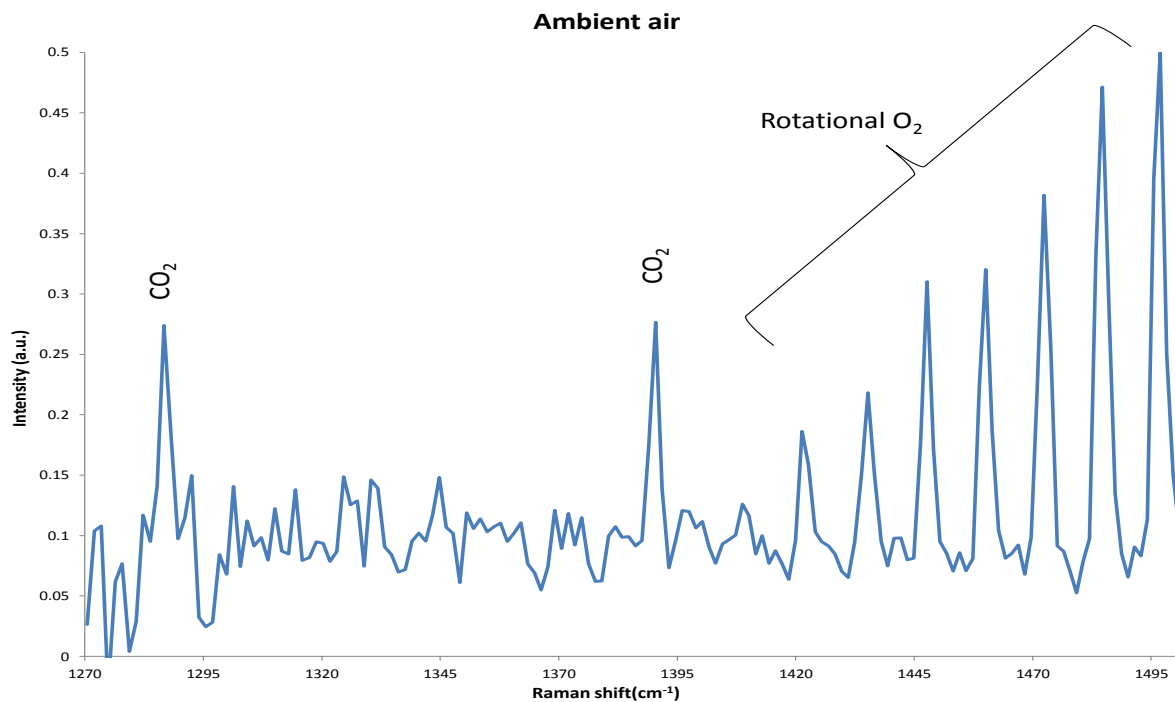


Figure 13 The measured spectrum of the ambient air by the Raman cell showing the Raman features of the carbon dioxide gas and a portion of the rotational oxygen lines

3.3 Signal-to-noise ratio

Figure 14 shows the enlarged spectrum focused on the carbon dioxide Raman peaks with error bars implemented. The experiment was repeated 150 times to obtain the spectrum with averaged intensity to reduce the statistical error. The error bars were assigned to this

spectrum based on the statistical variance of the 150 repeated spectra. The numerical variation of each pixel in the 150 repeated spectra for both the signal and background measurements were taken into account. These error bars may represent the fluctuation of the laser power within the measurement time frame and the error in counting statistics. The estimated signal-to-noise ratio of the carbon dioxide signal was ~ 14 , calculated by the averaged ratio of the signal strength of the two peaks to the respective statistical standard deviation. Using the signal-to-noise ratio obtained from the carbon dioxide peaks, assuming the minimum detectable signal to be the statistical variance of the spectrum (whose signal-to-noise ratio is equal to 1) and the equivalent measured concentration of the sample, the lower detection limit in this optical configuration is roughly 15 parts per million by volume (ppmv) of the carbon dioxide molecules under ambient conditions.

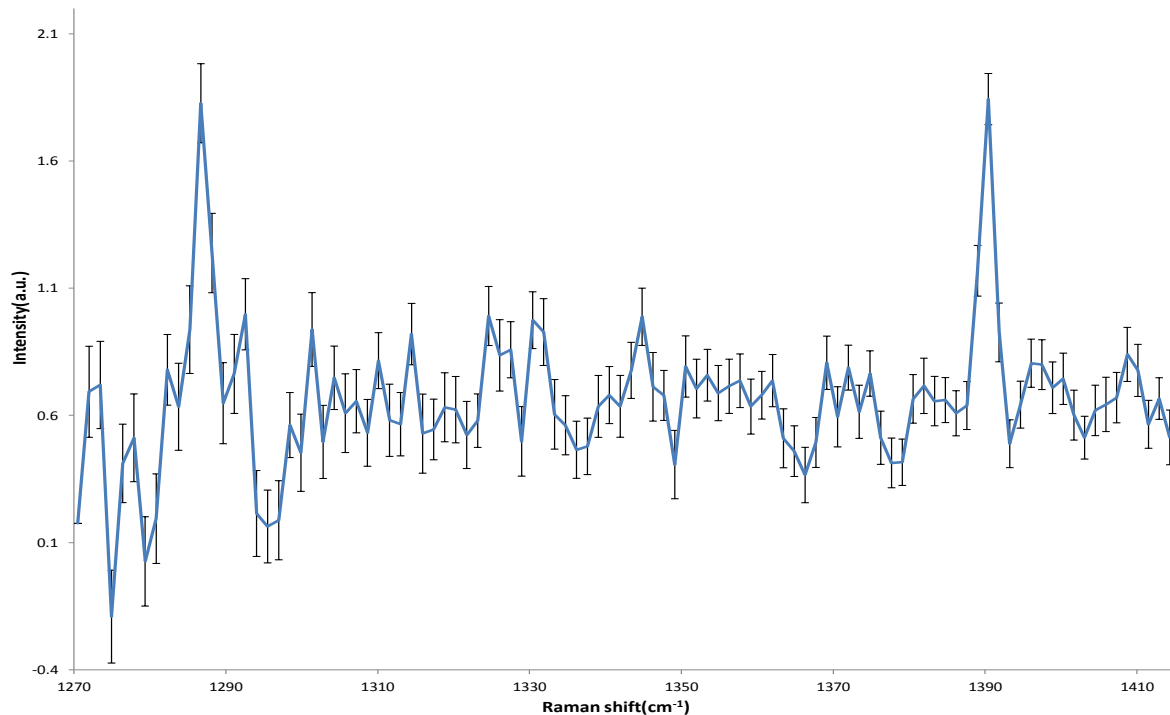


Figure 14 An enlarged Raman spectrum by the Raman cell showing the carbon dioxide features in the ambient air with error bars assigned

Chapter 4: Discussion and conclusion

In this chapter, the challenge and potential of this project are discussed and summarized to draw conclusions for the future studies. The performance of this Raman-gas cell based on a photonic crystal fibre is compared to the recent published Raman-gas cell based on a capillary hollow fibre. The future direction and improvements to ameliorate the performance of the system to detect analyte in ultra-trace amounts are discussed. The predicted challenges of breath analysis for clinical application are also discussed.

4.1 Comparison of a HC-PCF based Raman breath analyzer to that of based on a hollow capillary fibre

The HC-PCF based prototype was designed and developed at BC Cancer Research Centre in Vancouver, BC. The specifications and performance of this prototype were compared to another breath analyzer with a reflective material coated capillary fibre-based breath analyzer reported by Y.Okita et al (70), shown in Table 2. In this published experiment, a polycarbonate based hollow capillary optical fibre with a silver inner coating was employed to be the light guide and gas cell of the system. The excitation laser beam at 532 nm was focused to the inner silver coated capillary fibre (700 μm diameter) by a 70 mm focal length lens, while the other end of the fibre was opened. Back-scattered light (i.e., photons scattered in backward direction and traveling in the opposite direction to the incoming excitation laser) goes back by the original route. The laser beam was then collimated by the same focusing lens for filtering and re-focused to a Raman spectrometer for spectral analysis.

Attenuation: The internal silver coating helps to reduce attenuation loss of both the laser excitation and Raman signal. However, it is recommended to keep the capillary fibre straight in order to minimize the attenuation loss. This publication shows that the total power loss of this capillary fibre set-up (1.1 m long) can be up to more than 80% for the bending radius \sim 14 cm. This means that the strong attenuation of the inner silver coated capillary fibre due to bending would constrain the smallest possible size of the breath analyzer. In contrast, the HC-PCF typically has better optical guidance. The HC-PCF in this project (HC-800-01) has less than 10% loss per meter in attenuation within the transmission band of the fibre, and it is almost insensitive to bending. The experiment was run with a 2.5 m long HC-PCF coiled up onto a fibre wheel with a radius of a few centimeters.

Scattering modes: The back-scattered mode for Raman collection would theoretically give higher signal intensity, especially for fibres with strong attenuation, for example, capillary fibres. In contrast, both the laser and Stokes Raman photons had low attenuation in HC-800-01. Therefore, there should be no significant difference in terms of the Stokes Raman signal intensity in both forward- or back-scattered mode for fibre length less than \sim 5 m. The additional higher-order surface modes (considered as noise) decay exponentially in the cladding structure (74, 75) and therefore can be minimised in the forward-scattered mode. It was experimentally proven that forward-scattered mode can offer better signal-to-noise ratio over the back-scattered mode in this optical configuration.

Numerical aperture (NA): Hollow capillary fibres usually have low NA compared to the typical value of 0.22. This is because coupled light with high NA (small angle to the normal

line) would introduce extra absorption and scattering by the wall of the capillary and thus reduce reflection efficiency, which is governed by Fresnel's equation as a function of the incident angle. In this case, the focal length of the focusing lens has to be long enough to produce a low NA (since the NA is inversely proportional to the focal length of the lens). HC-800-01 has a NA ~ 0.2 , which does not require a lens with a particularly long focal length. The focusing lens used in this project was 18.4 mm, which is optimized for the coupling efficiency and the space taken by the gas chamber, in which it is ready for a compact design.

Detection limit: The detection limit of the capillary fibre-based system was roughly 0.2% (2000 ppmv equivalently) by extrapolating the Raman intensity as a function of the oxygen concentration to the measurable noise level, as the lowest measured concentration is $\sim 0.25\%$. The detection limit of this project for the HC-PCF-based breath analyzer was found by measuring the carbon dioxide level in air ($\sim 0.03\%$) and the statistical variance of 150 spectra. The detection limit of this single pass configuration was ~ 15 ppmv, which is over 100-fold improvement over the capillary system.

	BC Cancer Research Center	<i>Y. Okita et al</i>
Laser excitation wavelength	785 nm	532 nm
Fibre type	Hollow core photonic crystal fibre	Internal silver coated hollow capillary fibre
Fibre core	10 μm	700 μm
Fibre length	~ 2.5 m	1.1 m
Scattering mode	Forward	Backward
Bending	Coiled up (few cm radius)	Kept straight
Lowest concentration measured in air	$\sim 0.02\%$ by volume ^a	$\sim 0.25\%$ by volume
Detection limit	~ 15 ppmv	~ 2000 ppmv ^b

Table 2 Comparison between our HC-PCF-based Raman breath analyzer to that of based on a hollow capillary fibre reported by Y. Okita et al.

- a) *This is roughly 70% of the concentration of carbon dioxide gas in air, refer to section 3.2.2.*
- b) *The estimated detection limit based on an extrapolation of the Raman intensity as a function of the oxygen concentration.*

4.2 Future work to improve the device sensitivity

Most of the trace VOCs in exhaled breath are within the upper parts per billion by volume (ppbv) to the lower parts per trillion by volume (pptv) range. Isoprene, one of the potential lung cancer-related biomarkers in human exhaled breath, has concentrations on the order of magnitude of 10^2 ppbv. The Raman spectrum of isoprene has a very strong peak at 1638 cm^{-1} with cross-sections around 50 (76). To observe this peak from an exhaled breath sample, the Raman system has to have at least a single digit ppmv detection limit. In this case, it needs roughly 10-fold improvement over the sensitivity of the HC-PCF-based breath analyzer presented in this project. Possible improvements for the future work are discussed in this section.

Sample pre-concentration: Sample pre-concentration can artificially increase the concentration of particular types of analyte in a sample before the analytical procedure. Therefore, the signal-to-noise ratio and sensitivity of the device can be enhanced. This allows trace amounts of analyte with concentrations below the detection limit to possibly be detected. Solid-phase microextraction (SPME) is one of the pre-concentration tools used most frequently in VOC analysis (77-79). SPME contains a fibre that is adhesive to certain types of VOCs and the fibre can in principle adsorb targeted molecules based on the concentration proportion once the equilibrium is reached. Heating is then used to desorb the VOCs from the fibre. The fact that it is convenient and inexpensive allows researchers to selectively enhance the concentration of particular types of VOC. Sensitivity for certain VOCs in human breath can be further improved by integrating the low-temperature glassy

carbon with SPME (80). To make SPME useful in this project, a customized heating desorption chamber may be required to integrate it with the Raman-gas cell.

Interaction length: The Raman peak intensity depends on the number of successful Raman-scattered photons in the core of the HC-PCF. Excitation photons and sample molecules are confined in a tight space in the core of the fibre. One way to enhance the Raman intensity is to increase the length of the HC-PCF. This would increase the number of photon-molecule interactions in the fibre core and thus improve the signal strength with an optimal fibre length. Moreover, a multipass configuration (81) can also increase the effective interaction length by re-focusing the output excitation beam back into the Raman-gas cell such that the excitation beam can pass the Raman-gas cell back and forth multiple times to increase the number of Raman interactions. In this case, the photon-molecule interaction length can thus be enhanced to produce a better signal-to-noise ratio in a compact system.

Exposure time and statistical noise: The spectral signal-to-noise ratio of a Raman peak is a function of the exposure time. In Raman spectroscopy, the charge-coupled device (CCD) camera of the spectrometer introduces noise to each readout. By maximizing the exposure time in a single spectrum (the longest possible integration time before the CCD is saturated by the intensity of the peak of interest), the readout noise of the CCD camera can be minimized in each spectrum. On the other hand, the counting statistics error would also be introduced to each measurement. The counting statistics error can be minimized by repeating the experiment and averaging the collected spectral data. The averaged spectrum would represent values that are closer to the true mean in each pixel column of the camera. But the

statistical variance reduction would reach a plateau when the readout noise of the CCD becomes a dominant factor.

Laser power: The laser power is a measure of the number of photons in a laser beam in a given time frame. The larger the number of photons confined to the core of the fibre, the higher the chance of having more successful Raman scattering and propagate through the fibre. This HC-PCF can transmit high laser power with a good beam quality at a very high power density up to 10^{14} W/cm² (82). Therefore, employing a laser with higher power would be an alternative way to improve the sign-to-noise ratio.

4.3 Predicted challenges in breath analysis for clinical application

Researchers have been trying to make breath analysis more practical and applicable in clinical settings. However, the large variety of results in literature for the same test is one of the major problems preventing breath testing from being widely applied in the medical field. Source of predicted challenges and potential solutions in clinical application are discussed:

Mouth and nose exhalation: Researchers have demonstrated that concentration levels for some VOCs are affected by the route of exhalation, i.e., the mouth, nose or both. It was shown that some VOCs could be produced in the oral cavity instead of endogenously exchanged on the alveolar interface (83, 84). Therefore, the route of exhalation may affect the measured concentration of the analytes of interest.

Dead space air: Dead space air is the part of inhaled air which does not perform gas exchange, and it is usually the portion stays in the conducting airways during the breathing cycle. Breath sampling is a general sample of the exhaled breath and it is not easy to separate the dead space volume. The volume of breath samples from each patient can be different, therefore, the dead space volume can dilute the endogenous VOCs' concentration by different degrees. End tidal breath sampling (collection at the end of exhalation) for breath analysis is an interesting technique recently proposed. Certain target molecules from the end tidal breath would be less diluted by the dead space volume during the sampling. It has potential to provide an alternative pre-concentration method without chemical manipulation to the sample to avoid contamination and absorption competition. Researchers have shown the possibility of real-time buffered end tidal measurements of breath VOCs followed by MS-based techniques (85). Moreover, concentration of endogenous substances can vary considerably not only from person to person, but also day to day and even breath to breath for the same individual. Collection of breath sample can be done in a single breath but more accurate results can be done in averaging a series of breath samples (31).

Personal/medical issue: There is a lack of well-recognized standardization of endogenous VOCs' concentration profile in human exhaled breath. The difference in concentration level of some types of molecules can vary across gender, age, diet/eating habit, drug (86-88) or even the illness or disease. The fact that some patients are less able to offer full exhalation should be taken into account. For instance, patients with late-stage lung cancer may only be able to offer a small vital capacity due to the weak exhalation force. As inhaled air sitting at more upper airways would be exhaled before the lower airways, molecules released by a

deeper sitting tumour would be less exposed to the fresh air and less likely to be exhaled compared to those from the higher airways.

Measuring tools: To measure ultra-low concentrations, the testing tools must be cleaned and sterilized before use to remove potential contaminants, e.g., residues from the manufacturing process, cleaning agents, etc. To make sure the endogenous VOCs from the alveoli breath are measured and distinguished, some other common compounds that could be found in the oral cavity may also need to be eliminated during the analysis, e.g., oral hygiene products, food. Sample manipulation (such as pre-concentration) may also introduce calculation error due to the selective/non-linear absorption.

The combination of VOCs and their corresponding concentrations could vary significantly between different sample sources and instrumental responses. The background problem can generally be minimized by subtraction and supplying air for inhalation with known concentration of VOCs. However, these processes are less convincing if the concentration change of VOCs are tiny compared to the background level. Moreover, complex dependent issues are hard to be corrected for by a simple subtraction, such as the dead space volume. As a result of the above variances, data from breath analysis usually show wide variations. More effort has to be made in this area to provide adequate standardized procedure for breath sampling, analysis and background correction, to allow reliable comparison between different published results.

4.4 Conclusion

A Raman-gas cell based on HC-PCF for breath analysis has been designed and developed in the BC Cancer Research Centre in Vancouver, BC. This breath analyzer prototype based on photonics technology is potentially simpler, more cost-effective and faster than GC-MS. This Raman-gas cell contains two parts: optical and tubing system. The optical section contains a laser, optical fibres and other optical components. HC-800-01 is the HC-PCF used in this project and it serves as a light guide and gas cell. A tubing system was also constructed for the gas supply. In this project, Raman spectra from reference gases (oxygen gas, hydrogen gas, carbon dioxide gas) have been obtained. Human exhaled breath sample tests were also run to produce Raman spectrum for analysis. The experimental $eO_2:eCO_2$ concentration ratio was found to be almost 4:1. The detection limit of the system was found to be ~ 15 ppmv obtained from the averaged spectra of CO_2 in the ambient air. This is more than 100-fold improvement over the recent published results by a Raman-gas cell based on hollow capillary fibre. To be useful in testing molecules in the pptv to ppbv concentration range, the device sensitivity has to be improved in certain aspects such as: optimizing the interaction length of the fibre and possibly using a pre-concentration method to enhance signal-to-noise ratio.

Breath analysis is promising as a simple, painless and real-time testing method in the medical field. Exhaled VOCs are proven to be an indication of certain disease states, such as lung cancer. The photonics technique based breath analyzer can offer advantages in terms of compactness, affordability and multiplicity. This Raman-gas cell has great potential to be an inexpensive, non-invasive and point-of-care lung cancer screening tool to benefit our society.

References

1. Rizzo DC. Fundamentals of anatomy and physiology: Cengage Learning; 2009.
2. Shields TW, LoCicero J, Reed CE, Feins RH. General thoracic surgery: Lippincott Williams & Wilkins; 2009.
3. World Health Organization. Cancer fact sheet. 2012; Available from: <http://www.who.int/mediacentre/factsheets/fs297/en/>.
4. Siegel R, Ward E, Brawley O, Jemal A. Cancer statistics, 2011. CA: A Cancer Journal for Clinicians. 2011;61(4):212-36.
5. Rosti G, Bevilacqua G, Bidoli P, Portalone L, Santo A, Genestreti G. Small cell lung cancer. Ann Oncol. 2006;17(suppl 2):ii5-ii10.
6. Robert S. Porter M. The Merck manual of diagnosis and therapy: Wiley; 2011.
7. Khurana S. Lung cancer. South Asia Network for Chronic Disease.4.
8. Travis WD, Travis LB, Devesa SS. Lung cancer. Cancer. 1995;75(1 Suppl):191-202. Epub 1995.
9. Biesalski HK, De Mesquita BB, Chesson A, Chytil F, Grimble R, Hermus RJJ, et al. European consensus statement on lung cancer: risk factors and prevention. Lung cancer panel. CA: A Cancer Journal for Clinicians. 1998;48(3):167-76.
10. Vaporciyan AA NJ, Lee JS, et al. Cancer of the lung. Cancer Medicine. 2000;5th edition:Chapter 88. BC Decker.
11. Kumar V, Cotran RS, Robbins SL. Robbins basic pathology: Saunders; 2003.
12. Reed MF, Molloy M, Dalton EL, Howington JA. Survival after resection for lung cancer is the outcome that matters. The American Journal of Surgery. 2004;188(5):598-602.
13. World Health Organization. Screening and early detection of cancer. Available from: <http://www.who.int/cancer/detection/en/>.
14. Conrad DH, Goyette J, Thomas PS. Proteomics as a method for early detection of cancer: A review of proteomics, exhaled breath condensate, and lung cancer screening. J Gen Intern Med. 2008;23:78-84.
15. Bach PB, Kelley MJ, Tate RC, McCrory DC. Screening for lung cancer: a review of the current literature. Chest. 2003;123(1 Suppl):72S-82S. Epub 2003.
16. Thunnissen FBJM. Sputum examination for early detection of lung cancer. J Clin Pathol. 2003;56(11):805-10.
17. Kennedy TC, Lam S, Hirsch FR. Review of recent advances in fluorescence bronchoscopy in early localization of central airway lung cancer. Oncologist. 2001;6(3):257-62.
18. Patz EF, Goodman PC, Bepler G. Current concepts - Screening for lung cancer. New England Journal of Medicine. 2000;343(22):1627-33.
19. Read C, Janes S, George J, Spiro S. Early lung cancer: screening and detection. Primary Care Respiratory Journal. 2006;15(6):332-6.
20. Mukhopadhyay R. Don't waste your breath. Researchers are developing breath tests for diagnosing diseases, but how well do they work? Analytical chemistry. 2004;76(15):273A-6A. Epub 2004/08/26.
21. Phillips M. Breath tests in medicine. SciAm. 1992;267(1):74-9.

22. Rudnick SN, Milton DK. Risk of indoor airborne infection transmission estimated from carbon dioxide concentration. *Indoor Air*. 2003;13(3):237-45.
23. Risby TH, Solga SF. Current status of clinical breath analysis. *Applied Physics B- Lasers and Optics*. 2006;85(2-3):421-6.
24. Pauling L, Robinson AB, Teranish.R, Cary P. Quantitative analysis of urine vapor and breath by gas-liquid partition chromatography. *Proceedings of the National Academy of Sciences of the United States of America*. 1971;68(10):2374-&.
25. Phillips M, Herrera J, Krishnan S, Zain M, Greenberg J, Cataneo RN. Variation in volatile organic compounds in the breath of normal humans. *Journal of Chromatography B: Biomedical Sciences and Applications*. 1999;729(1-2):75-88.
26. Szulejko JE, McCulloch M, Jackson J, McKee DL, Walker JC, Solouki T. Evidence for cancer biomarkers in exhaled breath. *Sensors Journal, IEEE*. 2010;10(1):185-210.
27. Phillips M, Gleeson K, Hughes JMB, Greenberg J, Cataneo RN, Baker L, et al. Volatile organic compounds in breath as markers of lung cancer: a cross-sectional study. *Lancet*. 1999;353(9168):1930-3.
28. Manolis A. The diagnostic potential of breath analysis. *Clinical Chemistry*. 1983;29(1):5-15.
29. Sehnert SS, Jiang L, Burdick JF, Risby TH. Breath biomarkers for detection of human liver diseases: preliminary study. *Biomarkers : biochemical indicators of exposure, response, and susceptibility to chemicals*. 2002;7(2):174-87. Epub 2002.
30. Kneepkens CMF, Lepage G, Roy CC. The potential of the hydrocarbon breath test as a measure of lipid-peroxidation. *Free Radical Biology and Medicine*. 1994;17(2):127-60.
31. Miekisch W, Schubert JK, Noeldge-Schomburg GFE. Diagnostic potential of breath analysis - focus on volatile organic compounds. *Clinica Chimica Acta*. 2004;347(1-2):25-39.
32. Fens N, Zwinderman AH, van der Schee MP, de Nijs SB, Dijkers E, Roldaan AC, et al. Exhaled breath profiling enables discrimination of chronic obstructive pulmonary disease and asthma. *Am J Respir Crit Care Med*. 2009;180(11):1076-82. Epub 2009.
33. Critchley A, Elliott TS, Harrison G, Mayhew CA, Thompson JM, Worthington T. The proton transfer reaction mass spectrometer and its use in medical science: applications to drug assays and the monitoring of bacteria. *International Journal of Mass Spectrometry*. 2004;239(2-3):235-41.
34. Phillips M, Cataneo RN, Cummin ARC, Gagliardi AJ, Gleeson K, Greenberg J, et al. Detection of lung cancer with volatile markers in the breath. *Chest*. 2003;123(6):2115-23.
35. Bajtarevic A, Ager C, Pienz M, Klieber M, Schwarz K, Ligor M, et al. Noninvasive detection of lung cancer by analysis of exhaled breath. *BMC Cancer*. 2009;9(1):348.
36. Ligor M, Ligor T, Bajtarevic A, Ager C, Pienz M, Klieber M, et al. Determination of volatile organic compounds in exhaled breath of patients with lung cancer using solid phase microextraction and gas chromatography mass spectrometry. *Clinical Chemistry and Laboratory Medicine*. 2009;47(5):550-60.
37. Wehinger A, Schmid A, Mechtcheriakov S, Ledochowski M, Grabmer C, Gastl GA, et al. Lung cancer detection by proton transfer reaction mass-spectrometric analysis of human breath gas. *International Journal of Mass Spectrometry*. 2007;265(1):49-59.
38. Mazzone PJ. Analysis of volatile organic compounds in the exhaled breath for the diagnosis of lung cancer. *J Thorac Oncol*. 2008;3(7):774-80.

39. Poli D, Carbognani P, Corradi M, Goldoni M, Acampa O, Balbi B, et al. Exhaled volatile organic compounds in patients with non-small cell lung cancer: cross sectional and nested short-term follow-up study. *Resp Res.* 2005;6.
40. Chen X, Xu F, Wang Y, Pan Y, Lu D, Wang P, et al. A study of the volatile organic compounds exhaled by lung cancer cells in vitro for breath diagnosis. *Cancer.* 2007;110(4):835-44.
41. Poli D, Goldoni M, Caglieri A, Ceresa G, Acampa O, Carbognani P, et al. Breath analysis in non small cell lung cancer patients after surgical tumour resection. *Acta Biomed.* 2008;1:64-72.
42. Poli D, Goldoni M, Corradi M, Acampa O, Carbognani P, Internullo E, et al. Determination of aldehydes in exhaled breath of patients with lung cancer by means of on-fiber-derivatisation SPME-GC/MS. *Journal of Chromatography B-Analytical Technologies in the Biomedical and Life Sciences.* 2010;878(27):2643-51.
43. Song G, Qin T, Liu H, Xu G-B, Pan Y-Y, Xiong F-X, et al. Quantitative breath analysis of volatile organic compounds of lung cancer patients. *Lung Cancer.* 2010;67(2):227-31.
44. Mazzone PJ. Exhaled breath volatile organic compound biomarkers in lung cancer. *Journal of Breath Research.* 2012;6(2):027106.
45. Phillips M, Cataneo RN, Cummin AR, Gagliardi AJ, Gleeson K, Greenberg J, et al. Detection of lung cancer with volatile markers in the breath. *Chest.* 2003;123(6):2115-23. Epub 2003.
46. Machado RF, Laskowski D, Deffenderfer O, Burch T, Zheng S, Mazzone PJ, et al. Detection of lung cancer by sensor array analyses of exhaled breath. *American Journal of Respiratory and Critical Care Medicine.* 2005;171(11):1286-91.
47. McCulloch M, Jezierski T, Broffman M, Hubbard A, Turner K, Janecki T. Diagnostic accuracy of canine scent detection in early- and late-stage lung and breast cancers. *Integrative cancer therapies.* 2006;5(1):30-9.
48. Rieder J, Lirk P, Ebenbichler C, Gruber G, Prazeller P, Lindinger W, et al. Analysis of volatile organic compounds: possible applications in metabolic disorders and cancer screening. *Wien Klin Wochens.* 2001;113(5-6):181-5.
49. Davies S, Spanel P, Smith D. A new 'online' method to measure increased exhaled isoprene in end-stage renal failure. *Nephrology Dialysis Transplantation.* 2001;16(4):836-9.
50. Smith D, Turner C, Spanel P. Volatile metabolites in the exhaled breath of healthy volunteers: their levels and distributions. *Journal of Breath Research.* 2007;1(1).
51. Hansel A, Jordan A, Holzinger R, Prazeller P, Vogel W, Lindinger W. Proton-transfer reaction mass-spectrometry - online trace gas-analysis at the ppb level. *International Journal of Mass Spectrometry.* 1995;149:609-19.
52. Matthew RM, Yury B, Gerard W, Rafal L, Frank KT. Recent advances of laser-spectroscopy-based techniques for applications in breath analysis. *Journal of Breath Research.* 2007;1(1):014001.
53. Sigrist MW, Bartlome R, Marinov D, Rey JM, Vogler DE, Wachter H. Trace gas monitoring with infrared laser-based detection schemes. *Applied Physics B-Lasers and Optics.* 2008;90(2):289-300.
54. Wang C, Sahay P. Breath Analysis Using Laser Spectroscopic Techniques: Breath Biomarkers, Spectral Fingerprints, and Detection Limits. *Sensors.* 2009;9(10):8230-62.

55. Mazurenka M, Orr-Ewing AJ, Peverall R, Ritchie GAD. 4 Cavity ring-down and cavity enhanced spectroscopy using diode lasers. Annual Reports Section "C" (Physical Chemistry). 2005;101(001):100-42.
56. Paldus BA, Kachanov AA. An historical overview of cavity-enhanced methods. Canadian Journal of Physics. 2005;83(10):975-99.
57. Namjou K, Roller CB, McMillen G, editors. Breath-analysis using mid-infrared tunable laser spectroscopy. Sensors, 2007 IEEE; 2007 28-31 Oct. 2007.
58. Roller C, Namjou K, Jeffers J, Potter W, McCann PJ, Grego J. Simultaneous NO and CO₂ measurement in human breath with a single IV-VI mid-infrared laser. Opt Lett. 2002;27(2):107-9.
59. Pushkarsky MB, Webber ME, Patel CKN. Ultra-sensitive ambient ammonia detection using CO₂-laser-based photoacoustic spectroscopy. Applied Physics B-Lasers and Optics. 2003;77(4):381-5.
60. Czyzewski A, Ernst K, Karasinski G, Lange H, Rairoux P, Skubiszak W, et al. Cavity ring-down spectroscopy for trace gas analysis. Acta Phys Pol B. 2002;33(8):2255-65.
61. Singh R. C. V. Raman and the discovery of the Raman effect. Phys Perspect. 2002;4(4):399-420.
62. Shen YR, Bloembergen N. Theory of stimulated Brillouin and Raman scattering. Physical Review. 1965;137(6A):1787-&.
63. Rajagopal A. Modern Physics: Prentice-Hall Of India Pvt. Limited; 2004.
64. Schrader B. Infrared and Raman spectroscopy: Wiley; 2008.
65. Russell P. Photonic crystal fibers. Science. 2003;299(5605):358-62.
66. Russell PSJ. Photonic-crystal fibers. J Lightwave Technol. 2006;24(12):4729-49.
67. Méndez A, Morse TF. Specialty optical fibers handbook: Academic Press; 2007.
68. Penney CM, Lapp M. Raman-scattering cross-sections for water-vapor. Journal of the Optical Society of America. 1976;66(5):422-5.
69. Canadian Cancer Society. Canadian cancer statistics. 2012.
70. Okita Y, Katagiri T, Matsuura Y. A Raman cell based on hollow optical fibers for breath analysis. In: Gannot I, editor. Optical Fibers and Sensors for Medical Diagnostics and Treatment Applications X. Bellingham: SPIE-Int Soc Optical Engineering; 2010.
71. Fenner WR, Hyatt HA, Kellam JM, Porto SPS. Raman Cross-Section of Some Simple Gases. Journal of the Optical Society of America. 1973;63(1):73-7.
72. Barrett JJ, Adams III NI. Laser-excited rotation-vibration Raman scattering in ultra-small gas samples. J Opt Soc Am. 1968;58(3):311-8.
73. Hoskins LC. Pure rotational Raman-spectroscopy - dry-lab experiment. J Chem Educ. 1977;54(10):642-3.
74. West JA, Smith CM, Borrelli NF, Allan DC, Koch KW. Surface modes in air-core photonic band-gap fibers. Optics Express. 2004;12(8):1485-96.
75. Wilding NV, Light PS, Couny F, Benabid F. Experimental comparison of electromagnetically induced transparency in acetylene-filled kagome and triangular lattice hollow core photonic crystal fiber. 2008 Conference on lasers and electro-optics & quantum electronics and laser science conference, Vols 1-9. 2008:1953-4.
76. Trulson MO, Mathies RA. Excited-state structure and dynamics of isoprene from absolute resonance Raman intensities. The Journal of Physical Chemistry. 1990;94(15):5741-7.

77. Grote C, Pawliszyn J. Solid-phase microextraction for the analysis of human breath. *Analytical chemistry*. 1997;69(4):587-96. Epub 1997.
78. Yu H, Xu L, Wang P. Solid phase microextraction for analysis of alkanes and aromatic hydrocarbons in human breath. *Journal of chromatography B, Analytical technologies in the biomedical and life sciences*. 2005;826(1-2):69-74. Epub 2005.
79. Hyspler R, Crhova S, Gasparic J, Zadak Z, Cizkova M, Balasova V. Determination of isoprene in human expired breath using solid-phase microextraction and gas chromatography-mass spectrometry. *Journal of chromatography B, Biomedical sciences and applications*. 2000;739(1):183-90. Epub 2000/04/01.
80. Giardina M, Olesik SV. Application of low-temperature glassy carbon-coated macrofibers for solid-phase microextraction analysis of simulated breath volatiles. *Analytical chemistry*. 2003;75(7):1604-14.
81. Altkorn R, Malinsky MD, Van Duyne RP, Koev I. Intensity considerations in liquid core optical fiber Raman spectroscopy. *Applied Spectroscopy*. 2001;55(4):373-81.
82. Ishaaya AA, Hensley CJ, Shim B, Schrauth S, Koch KW, Gaeta AL. Highly-efficient coupling of linearly- and radially-polarized femtosecond pulses in hollow-core photonic band-gap fibers. *Optics Express*. 2009;17(21):18630-7.
83. Wang TS, Pysanenko A, Dryahina K, Spanel P, Smith D. Analysis of breath, exhaled via the mouth and nose, and the air in the oral cavity. *Journal of Breath Research*. 2008;2(3).
84. Pysanenko A, Spanel P, Smith D. A study of sulfur-containing compounds in mouth- and nose-exhaled breath and in the oral cavity using selected ion flow tube mass spectrometry. *Journal of Breath Research*. 2008;2(4).
85. Herbig J, Titzmann T, Beauchamp J, Kohl I, Hansel A. Buffered end-tidal (BET) sampling-a novel method for real-time breath-gas analysis. *Journal of Breath Research*. 2008;2(3).
86. Spanel P, Dryahina K, Smith D. The concentration distributions of some metabolites in the exhaled breath of young adults. *Journal of Breath Research*. 2007;1(2).
87. Smith D, Spanel P, Davies S. Trace gases in breath of healthy volunteers when fasting and after a protein-calorie meal: a preliminary study. *Journal of Applied Physiology*. 1999;87(5):1584-8.
88. Epton MJ, Ledingham K, Dummer J, Hu WP, Rhodes B, Senthilmohan ST, et al. Interference of chlorofluorocarbon (CFC)-containing inhalers with measurements of volatile compounds using selected ion flow tube mass spectrometry. *Rapid Communications in Mass Spectrometry*. 2009;23(3):443-7.